AGU PUBLICATIONS

JGR

Journal of Geophysical Research: Solid Earth

RESEARCH ARTICLE
10.1002/2016JB013451

Key Points:
- 3-D imaging of a fault-controlled basin architecture via time domain electromagnetic and ambient vibration surveys
- Complex subsurface architecture characterized by buried faults and depocenters separated by thresholds
- Insights into the long-term Paganica-San Demetrio Fault System evolution and behavior (2009 L'Aquila earthquake fault)

Supporting Information:
- Supporting Information S1
- Table S1

Correspondence to:
R. Civico,
riccardo.civico@ingv.it

Citation:
Civico, R., et al. (2017), Geometry and evolution of a fault-controlled Quaternary basin by means of TDEM and single-station ambient vibration surveys: The example of the 2009 L'Aquila earthquake area, central Italy, *J. Geophys. Res. Solid Earth*, *122*, doi:10.1002/2016JB013451.

Received 1 AUG 2016
Accepted 7 MAR 2017
Accepted article online 10 MAR 2017

Geometry and evolution of a fault-controlled Quaternary basin by means of TDEM and single-station ambient vibration surveys: The example of the 2009 L'Aquila earthquake area, central Italy

R. Civico[1], V. Sapia[1], G. Di Giulio[2], F. Villani[2], S. Pucci[1], P. Baccheschi[1], S. Amoroso[2], L. Cantore[2], D. Di Naccio[2], S. Hailemikael[3], A. Smedile[1], M. Vassallo[2], M. Marchetti[1], and D. Pantosti[1]

[1]Istituto Nazionale di Geofisica e Vulcanologia, Rome, Italy, [2]Istituto Nazionale di Geofisica e Vulcanologia, L'Aquila, Italy, [3]ENEA, Rome, Italy

Abstract We applied a joint survey approach integrating time domain electromagnetic soundings and single-station ambient vibration surveys in the Middle Aterno Valley (MAV), an intermontane basin in central Italy and the locus of the 2009 L'Aquila earthquake. By imaging the buried interface between the infilling deposits and the top of the pre-Quaternary bedrock, we reveal the 3-D basin geometry and gain insights into the long-term basin evolution. We reconstruct a complex subsurface architecture, characterized by three main depocenters separated by thresholds. Basin infill thickness varies from ~200–300 m in the north to more than 450 m to the southeast. Our subsurface model indicates a strong structural control on the architecture of the basin and highlights that the MAV experienced considerable modifications in its configuration over time. The buried shape of the MAV suggests a recent and still ongoing predominant tectonic control by the NW-SE trending Paganica-San Demetrio Fault System (PSDFS), which crosscuts older ~ENE and NNE trending extensional faults. Furthermore, we postulate that the present-day arrangement of the PSDFS is the result of the linkage of two previously isolated fault segments. We provide constraints on the location of the southeastern boundary of the PSDFS, defining an overall ~19 km long fault system characterized by a considerable seismogenetic potential and a maximum expected magnitude larger than *M* 6.5. This study emphasizes the benefit of combining two easily deployable geophysical methods for reconstructing the 3-D geometry of a tectonically controlled basin. Our joint approach provided us with a consistent match between these two independent estimations of the basin substratum depth within 15%.

1. Introduction

The central Apennines of Italy are one of the most seismically active areas in the Mediterranean region, as highlighted by the occurrence of repeated strong earthquakes in the past [*Valensise and Pantosti*, 2001] and by the presence of a large number of active faults that play a primary role in shaping the present landscape of the mountain chain. Active extensional tectonics controls many tectonic intermontane basins bounded by seismogenic normal faults (e.g., the Gubbio, Norcia, Castelluccio, Rieti, Sulmona, and Fucino basins). The presence of flat areas, within otherwise steep and rough slopes, favored the development of important historical settlements in the past and promoted dense urbanization in recent times. The closeness of these developments to active, seismogenic faults is the basis of a high exposure to seismic risk for tens of thousands of people, industrial centers, power plants, and invaluable historical/cultural heritage sites.

Among other factors, key elements that may help to mitigate the seismic risk and allow sustainable use of the territory, preservation of the building heritage, and of the infrastructure, are (1) a thorough understanding of the seismic behavior of active normal faults in time and space and (2) a reconstruction of the local geological and geotechnical characteristics that may have an impact on seismic ground motions and their local amplifications.

The basin geometry at depth, sedimentary facies, and depositional architecture reflect the style and rate of long-term deformation related to the activity of the bounding normal fault system [*Leeder and Gawthorpe*, 1987; *Westaway*, 1991; *Nicol et al*., 1997; *Gawthorpe and Leeder*, 2000]. Therefore, a 3-D image of the fault-related basin structure and infill can represent a synopsis of its tectonic evolution through time that can be used to infer the fault seismic behavior and possibly forecast its future activity. This is particularly true

in continental environments, where uplifted footwall blocks promote erosion of key depositional and morphological markers of deformation that are buried and preserved in the downthrown hanging wall.

Furthermore, the 3-D basin imaging allows us to define the infill geometry and thickness changes; this is crucial for scenario-based seismic hazard analyses, because wave reverberation and local ground-motion amplification are primarily controlled by sharp seismic velocity contrasts, geometric complexities in the buried bedrock topography, and lithological properties of the sedimentary infill [*Bard and Bouchon*, 1980; *Aki*, 1988; *De Luca et al*., 2005; *Hartzell et al*., 2016; among many others]. In fact, increased duration, frequency-dependent ground-motion amplification, and spatial variability of ground motions have been observed frequently in both the near- and far-field of strong to great earthquakes. Among many other cases, large amplifications and very long time durations were observed in 1985 in Mexico City after the two destructive earthquakes (magnitudes $M_S = 8.1$ and $M_S = 7.5$) which occurred off the Pacific coast (nearly 400 km away) [*Flores-Estrella et al*., 2006].

The M_w 6.1 6 April 2009 main shock in central Italy and its several monthlong aftershock sequence [*Scognamiglio et al*., 2010; *Herrmann et al*., 2011] are an expression of all that we discussed above: (1) they hit a densely populated area in the Middle Aterno Valley (hereinafter the MAV), one of the main fault-controlled basins in the central Apennines, and caused 309 fatalities and thousands of injuries, as well as heavy damage to the town of L'Aquila (~80,000 inhabitants) and surrounding villages; (2) they occurred in an area repeatedly struck by several damaging earthquakes in the past (http://emidius.mi.ingv.it/CPTI) [*Tertulliani et al*., 2009; *Rovida et al*., 2011] that likely contributed to the growth and evolution of the basin (Figure 1); and (3) they produced large variations in local site response to ground shaking due to the deep geometry of the basin and variations in the thickness and type of basin-filling sediments [*Santucci de Magistris et al*., 2013].

Prior to the 2009 event, the overall deep geometry of the MAV, the structural setting, and the long-term activity of the earthquake causative fault (the Paganica-San Demetrio Fault System (PSDFS)) were only roughly defined (see *Galli et al*. [2010] for a review). The seismic event of 2009 promoted numerous studies, focusing mainly on the local structural setting, on the analysis of the Quaternary geological and morphological expression of the PSDFS, and on its paleoseismic history [*Galli et al*., 2010, 2011; *Cinti et al*., 2011; *Giaccio et al*., 2012; *Lavecchia et al*., 2012; *Blumetti et al*., 2013; *Moro et al*., 2013; *Civico et al*., 2015; *Pucci et al*., 2015].

In only a few studies the shallow subsurface of the MAV and its relation to the PSDFS have been investigated. These works were performed mainly in the northwestern sector of the basin, in the epicentral area of the 2009 main shock [*Cesi et al*., 2010; *Balasco et al*., 2011; *Giocoli et al*., 2011; *Improta et al*., 2012; *Tallini et al*., 2012; *Pucci et al*., 2016; *Macrì et al*., 2016; *Villani et al*., 2017]. Worthy of note, deep boreholes and seismic exploration lines from the oil and gas industry are lacking in this area, thus hampering a basin-scale knowledge of the subsurface setting. The above mentioned studies provided some clues on the subsurface basin geometry; however, these results have not produced an overall 3-D image because of (1) the lack of quantitative data on the basin infill [*Cesi et al*., 2010] or (2) because measurements were performed along localized 2-D sections [*Balasco et al*., 2011; *Giocoli et al*., 2011; *Improta et al*., 2012; *Pucci et al*., 2016], and their investigated area is quite limited compared to the $>100\,km^2$ extent of the MAV.

Given the poor knowledge of the 3-D architecture of the MAV and a more general motivation of providing a methodology to reconstruct the evolution of a fault-controlled basin, we chose to integrate two different easily deployable, inexpensive, and reliable geophysical methods: time domain electromagnetic soundings (hereinafter TDEM) and single-station ambient vibration recordings analyzed by the horizontal-to-vertical spectral ratio method (hereinafter H/V). TDEM and H/V surveys were used in the MAV to image the top of the Mesozoic-Cenozoic substratum and were integrated with a revised set of existing boreholes and other geophysical data collected during seismic microzonation studies following the 2009 L'Aquila earthquake [*MS-AQ Working Group*, 2010], as well as with the findings of recent works performed in the area [*Improta et al*., 2012, *Di Giulio et al*., 2014; *Villani et al*., 2015, 2017].

This paper is organized as follows: we first briefly present the seismotectonic setting of the MAV in the context of the 2009 L'Aquila earthquake, a review of the preexisting knowledge on the subsurface setting of the MAV from available geophysical investigations, and the applied methodology and the survey strategy. We then describe the results of this work, providing a smooth and comprehensive 3-D subsurface image of

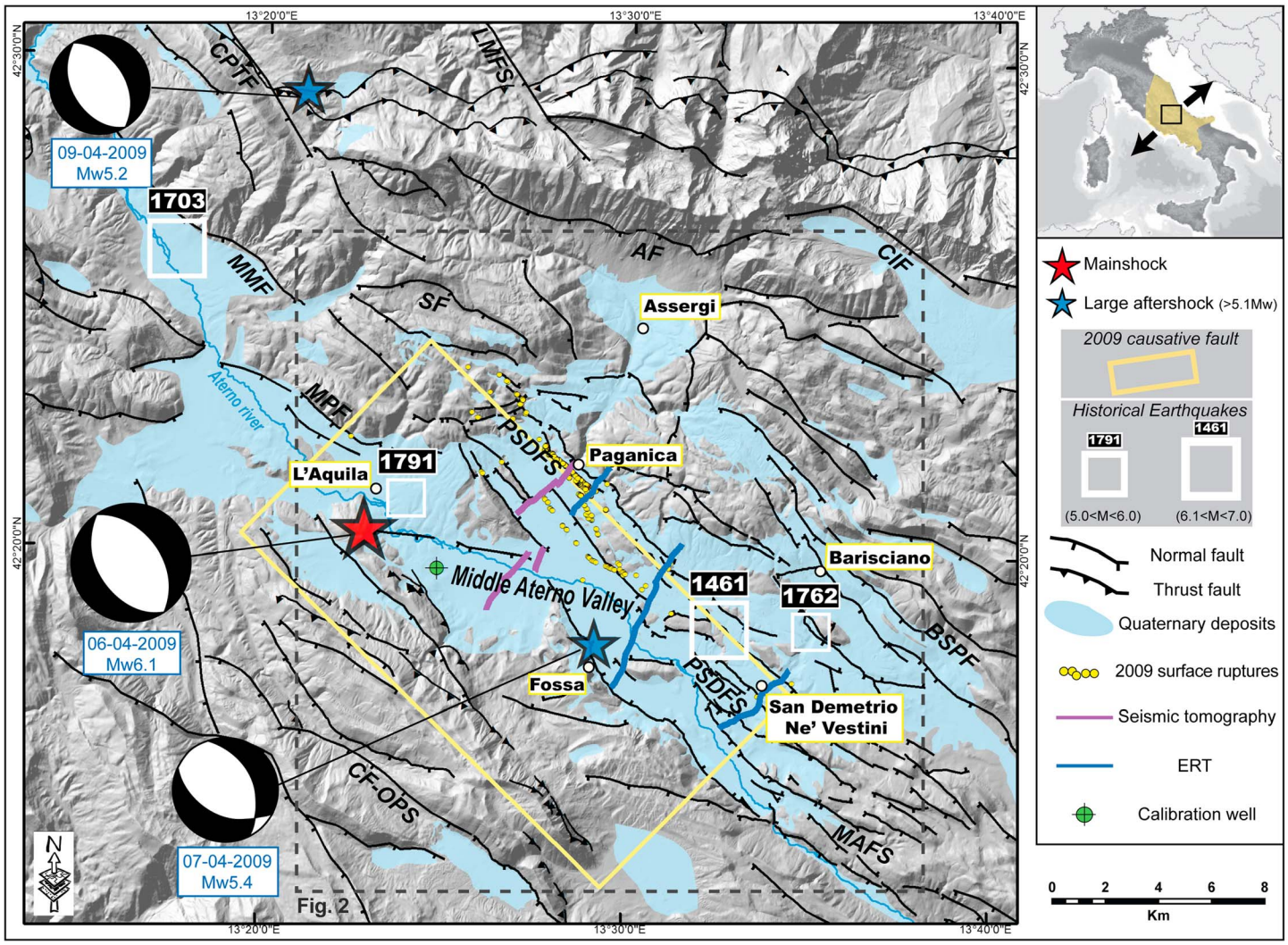

Figure 1. Location map of the 2009 L'Aquila main shocks ($M > 5.0$; stars) [*Scognamiglio et al*., 2010; *Herrmann et al*., 2011]. Focal mechanisms of the main shock and of the two largest aftershocks, historical seismicity ($M > 5.0$; http://emidius.mi.ingv.it/CPTI04), and main active faults are shown (acronyms as follows: CPTF: Capitignano Fault, MMF: Mount Marine Fault, SF: Stabiata Fault, LMFS: Laga Mountain Fault System, AF: Assergi Fault, CIF: Campo Imperatore Fault, MPF: Mount Pettino Fault, PSDFS: Paganica - San Demetrio Fault System, BSPF: Barisciano-San Pio Fault, MAFS: Middle Aterno Fault System, CF-OPS: Campo Felice-Ovindoli Pezza Fault System [modified after *Galadini and Galli*, 2000; *Civico et al*., 2015; *Pucci et al*., 2015]). The yellow box is the approximate projection to the surface of the ~19 km long 2009 main shock causative fault according to several investigators (see a review in *Vannoli et al*. [2012] and in *Chiaraluce* [2012]). The traces of the seismic tomography profiles [*Improta et al*., 2012; *Villani et al*., 2017] and of the ERT (electrical resistivity tomography) investigations [*Pucci et al*., 2016] are reported. The inset shows the direction of extension across the central Apennines (black arrows), and the regional felt area for the 6 April main shock according to www.haisentitoilterremoto.it (colored area).

the MAV. Finally, we discuss our main findings in terms of (1) the relations between the subsurface geometry, the structural arrangement, and the Quaternary basin evolution and (2) the seismotectonic- and seismic hazard-related implications of this work. At the same time, we present an example of the joint use of the TDEM and H/V method combined approach that can be applied to the exploration of other areas with similar geological settings and prone to significant seismic hazard.

2. Geological Setting and Quaternary Tectonic Framework

Since the late Pliocene, active normal faulting has superimposed and dissected a previously shortened continental crust, which now forms the NE verging central Apennines thrust-and-fold belt [e.g., *Lavecchia et al*., 1994; *Galadini and Galli*, 2000; *Galadini and Messina*, 2004; *Boncio et al*., 2004]. Whereas thrusting continues to

the present day on the Adriatic side of the Apennines, NE trending contraction within the axial portion of the chain ceased in between late Miocene and early Pliocene [*Patacca et al*., 1990]. The present-day extension is perpendicular to the chain axis [*Montone et al*., 2012, and references therein] and is estimated to be 2–3 mm/yr [*Hunstad et al*., 2003; *D'Agostino et al*., 2011]. Pliocene-Quaternary extension generated a network of 15–35 km long, mainly NW-SE trending, SW dipping normal or transtensional active fault systems composed of shorter (typically 2–7 km long) interconnected individual splays [*Galadini and Galli*, 2000; *Cowie and Roberts*, 2001], but locally also promoted the reactivation of preexisting cross structures [*Pizzi and Galadini*, 2009]. NE-SW active extension is also confirmed by a diffuse upper crustal seismicity (epicentral depths up to 12–15 km [*Bagh et al*., 2007]), with episodic large ($M > 6$) earthquakes [*Chiarabba et al*., 2005; *Rovida et al*., 2011]. Several intermontane basins, filled with sequences of Plio-Quaternary continental deposits up to hundreds of meters in thickness, developed in the hanging wall of the NW-SE trending, SW dipping normal faults [*Cavinato and De Celles*, 1999; *Bosi et al*., 2003; *Galli et al*., 2010; *Giaccio et al*., 2012; *Pucci et al*., 2015; among many others].

The 2009 L'Aquila seismic sequence is consistent with these geologic and seismotectonic contexts. The seismologic, geodetic, differential interferometric synthetic aperture radar, and geological data concur with there being a NW-SE oriented, SW dipping tectonic structure as the M_w 6.1 6 April 2009 main shock causative fault (yellow box in Figure 1) [*Chiaraluce*, 2012; *Vannoli et al*., 2012, and references therein], which coincides with the ~19 km long network of normal faults bounding the MAV to the NE, known as the Paganica-San Demetrio Fault System (PSDFS) (in the sense of *Civico et al*. [2015]). During the 6 April main shock, this fault caused a coseismic surface displacement clearly observed for a minimum total length of ≥3 km (Figure 1) and consists of a complex set of small scarps (up to 0.15 m high) and open cracks [*Emergeo Working Group*, 2010; *Vittori et al*., 2011].

The PSDFS is characterized by a complex surface expression, with several synthetic and antithetic splays affecting the Quaternary basin continental infill [*Bagnaia et al*., 1992; *Vezzani and Ghisetti*, 1998; *Boncio et al*., 2004; *Istituto Superiore per la Protezione e la Ricerca Ambientale (ISPRA)*, 2006; *Civico et al*., 2015; *Pucci et al*., 2015] (Figure 1). The long-term Quaternary activity of the PSDFS generated the wide basin known as the Paganica-San Demetrio Basin (hereinafter the PSDB) that along with the nearby Bagno Basin constitutes the MAV (Figure 2).

The physiography of the PSDB and the Bagno Basin is dominated by the presence of the Aterno River, flowing roughly from the NW to the SE. The average elevation of the Bagno Basin floodplain is around 590–585 m above sea level (asl), whereas the PSDB floodplain elevation varies between 625 and 555 m asl. The southern portion of the PSDB (San Demetrio ne' Vestini area) is characterized by an exhumed Quaternary basin and by a staircase landscape, with both erosional and depositional flat surfaces that lie at different elevations with respect to the present-day basin floor [*Pucci et al*., 2015]. Moreover, this area is characterized by the occurrence of several intrabasin bedrock highs (i.e., Cerro, La Petrara, and S. Giovanni hills; Figure 2). The extent of the present-day PSDB is limited by the presence of an incised bedrock threshold, located close to Campana village, standing at an elevation of ~555 m asl (Figure 2).

The Quaternary infill of the PSDB and of the Bagno Basin exhibits complex stratigraphical relationships (including large unconformities and hiatuses) and unconformably overlies a Meso-Cenozoic marine substratum (Figure 2) [*Bertini and Bosi*, 1993; *D'Agostino et al*., 1997; *Cavinato and De Celles*, 1999; *ISPRA*, 2006; *Giaccio et al*., 2012; *Pucci et al*., 2015]. The latter is mainly composed of marly-carbonate marine sequences, and, to a lesser extent, by Miocene calcareous-arenaceous flysch (Bagno area [*ISPRA*, 2006]).

The thickness of the outcropping Quaternary continental sequence is ~100 m, whereas its compound maximum thickness, inferred from stratigraphical correlations between different sectors of the basin, attains ~400 m [*Pucci et al*., 2015]. According to *Giaccio et al*. [2012], the Quaternary continental deposits in the PSDB can be referred to three main unconformity-bounded fluvio-lacustrine synthemes: (1) a lower fluvio-lacustrine syntheme (early Pleistocene), made of lacustrine silts and of alluvial fan conglomerates and breccias, which represents the largest and most widespread Quaternary sedimentary unit; (2) an upper alluvial syntheme (middle Pleistocene), consisting of fluvial gravels, silts, and sands; and (3) a late fluvial-alluvial syntheme (middle/late Pleistocene to Present), consisting of fluvial/alluvial sandy-gravelly sediments, mainly related to the Aterno and Raiale Rivers. Notably, a generalized southward increase in thickness of the infilling deposits is observed moving from the Paganica area to the San Demetrio ne' Vestini area.

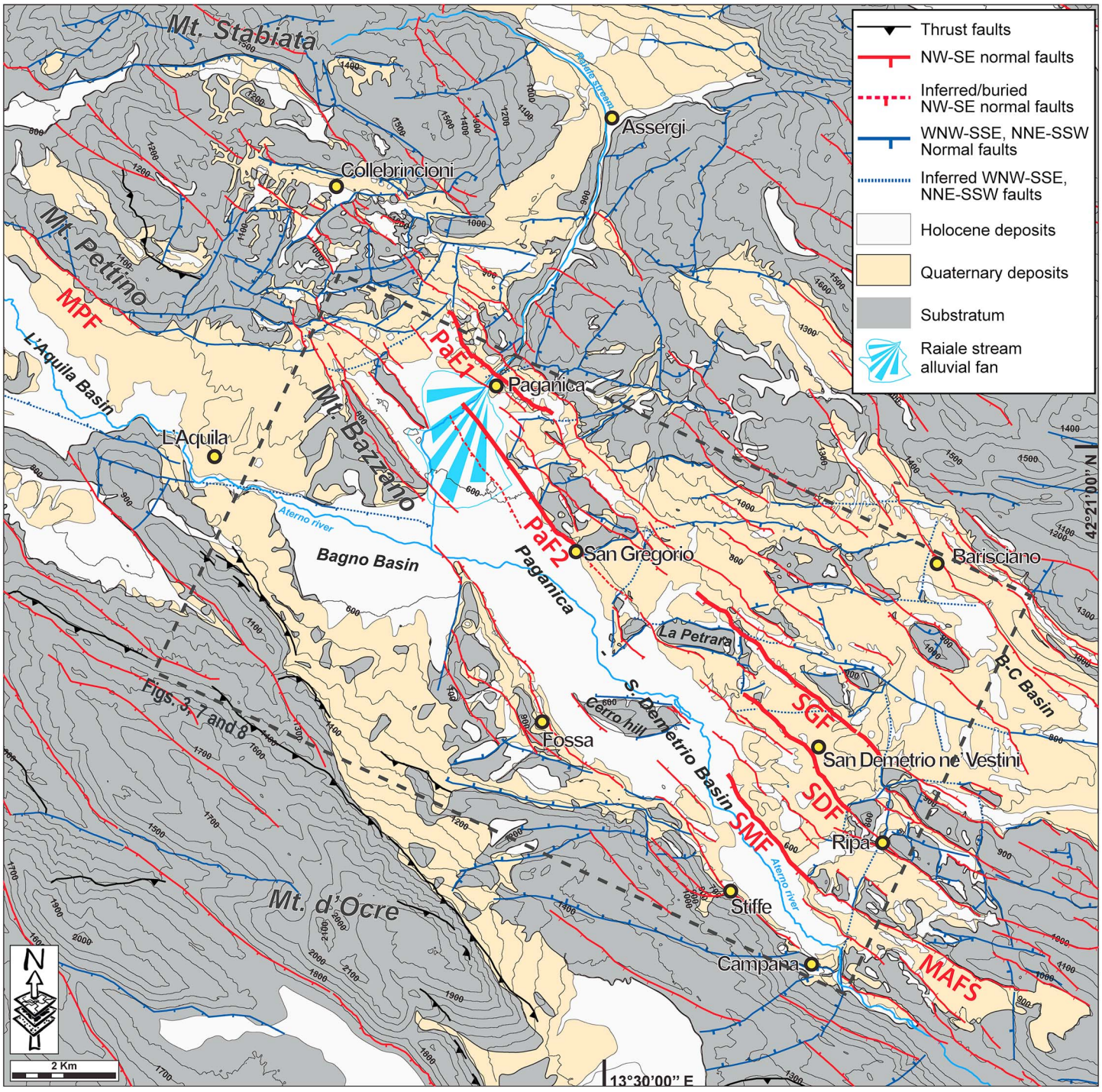

Figure 2. Simplified geologic map of the Paganica-San Demetrio and Bagno basins area, highlighting the architecture of the fault system at surface and the outcropping pre-Quaternary, Quaternary and Holocene deposits - modified after *Pucci et al*. [2014]. Major faults relevant to this study: MPF, Mount Pettino fault; PaF1, Paganica fault; PaF2, San Gregorio splay of the Paganica Fault; SGF, San Giovanni fault; SDF, San Demetrio Fault; SMF, San Mauro Fault; MAFS, Middle Aterno fault system. PaF1, PaF2, SGF, SDF, and SMF are part of the PSDFS.

The stratigraphic sequence of the Bagno Basin is less well defined. A recent ~150 m deep borehole (LAQUICORE [*Porreca et al*., 2016; *Macrì et al*., 2016]), although not reaching the pre-Quaternary basement, provided new constraints on the architecture of the subsurface Quaternary continental deposits. According to this work, the Bagno Basin is characterized by two main sequences separated by a gravel package occurring

between 84 and 115 m of depth: (1) an upper fluvial-alluvial sequence, and (below 41 m) palustrine sediments Middle Pleistocene-Holocene in age, and (2) an early Pleistocene lower palustrine sequence.

As for the structural setting of the MAV area, the NW striking PSDFS bounds the north-eastern margin of the PSDB. Several authors constrained the PSDFS length taking into account the sharp bend of the bounding main fault traces south of Collebrincioni village, to the north (step with the Mount Pettino Fault (MPF) in Figure 2), and the step over relation with the Middle Aterno Fault System (MAFS) to the south [*Boncio et al*., 2004], defining an overall ~19 km long fault system [*Cinti et al*., 2011; *Giaccio et al*., 2012; *Blumetti et al*., 2013; *Civico et al*., 2015]. Recently, detailed mapping of the PSDFS [*Civico et al*., 2015; *Pucci et al*., 2015] highlighted a complex surface expression of Quaternary faulting, consisting of several, closely spaced synthetic and antithetic splays, mostly NW striking and affecting the bedrock and the Quaternary deposits (Figure 2). According to these two studies, the PSDFS includes two main sectors: (1) the Paganica sector to the northwest, characterized by a relatively narrow deformation zone and a small Quaternary basin, and (2) the San Demetrio ne' Vestini sector to the southeast, characterized by an array of parallel fault splays and by a wider Quaternary basin. The most relevant fault segments of the PSDFS (Figure 2) are (1) the Paganica Fault (PaF), which comprises two main splays in the Paganica and S. Gregorio village areas (PaF1 and PaF2, respectively), (2) the San Giovanni Fault (SGF), (3) the San Demetrio Fault (SDF), and (4) the San Mauro Fault (SMF). The western side of the PSDB is flanked by Mount Bazzano and the Fossa-Stiffe ridge, controlled by a single compound alignment of NE dipping high-angle faults. On the basis of the long-term morphologic displacement pattern, *Civico et al*. [2015] infer that the PSDFS behaves as an individual extensional SW dipping seismogenic fault, capable of generating up to *M* 6.6 earthquakes.

In the study area, few compressional structures are well exposed. The most important thrust structures are represented by the E-W Gran Sasso thrust to the north [*Ghisetti and Vezzani*, 1991; *Adamoli*, 1992] and the NW trending Mount D'Ocre thrust-system [*ISPRA*, 2006] to the south, displaying north and north-east general vergence, respectively. The substratum bounding the PSDB does not show major thrusts and is typically characterized by gentle, open folds.

The overall structural setting of the MAV area is even more complex due to the presence of NNE and WNW trending extensional systems (Figure 2): *Pucci et al*. [2014] interpret that these two fault sets due to the reactivation with normal-oblique kinematics of previous conjugate strike-slip systems (E-W trending, mostly left-lateral and NNE-SSE right-lateral faults) have possibly developed during the compressional phase. Moreover, the Authors state that these faults may be responsible for the occurrence of the aforementioned intrabasin bedrock highs.

3. Previous Geophysical Investigations

The complex surficial stratigraphic and structural setting at the basin scale is also reflected in the subsurface setting. *Cesi et al*. [2010] produced a residual gravimetric anomaly map of the MAV (Figure 7b). This image suggests a complex structure for the entire basin, but it does not provide quantitative clues regarding the variable infill thickness because calibration with density data and forward modeling of the gravimetric anomalies have not yet been performed. *Balasco et al*. [2011] investigated the subsurface structure of the MAV by means of an ~8 km long, ~1000 m deep electrical resistivity tomography (ERT) survey performed in the northwestern sector of the basin. They highlighted the existence of areas of complex lateral and vertical heterogeneity in resistivity between Mount Bazzano and Paganica, interpreted as being due to a shallow conductive alluvial fill (up to 200 m thick) above the carbonate substratum. A narrow depocenter of low-resistivity sediments in the hanging wall and close to the Paganica Fault was defined too. Further, *Improta et al*. [2012] performed an ~8 km long 2-D shallow seismic survey across the northern part of the PSDB and in the Bagno Basin, in the hanging wall of the PSDFS (Figure 1). Their tomographic sections imaged a dissected pre-Quaternary substratum, with a main ~250 m deep depocenter in the Mount Bazzano fault hanging wall. Moreover, they evidenced the presence of lateral heterogeneities and steps in the substratum, compatible with the presence of buried fault splays of the PSDFS dissecting both the bedrock and the basin infill deposits. More recently, *Villani et al*. [2017] have expanded the seismic exploration within the Paganica basin, and their results reveal that the hanging wall of the PaF is characterized by the occurrence of several previously unreported splays active during the Quaternary: overall, the extensional fault system within the

Paganica sector accrued about 650 m net displacement, with a resultant minimum long-term Quaternary slip rate of 0.30 mm/yr.

Pucci et al. [2016] presented the results of three 2-D deep ERT transects, up to 6.36 km long, across the PSDB (see Figure 1 for location). The obtained resistivity models suggested the existence of several tectonic features that displaced the Meso-Cenozoic substratum, producing buried landforms and depressions, filled with Plio-Quaternary continental deposits. ERT results indicate that the basin bottom reaches a depth of about 600 m toward the south in the area of San Demetrio ne' Vestini, with the maximum continental infill exceeding the known thickness of the outcropping Quaternary sequence (about 400 m). The geological interpretation of the ERT images shows a structural style consisting of SW dipping normal faults, from which NE dipping antithetic faults splay out defining grabens acting as sedimentary traps. Moreover, *Pucci et al*. [2016] identified the location of the most active faults as leading splays of the 2009 earthquake causative fault system; these are Fault Zone 2 in the Paganica and San Gregorio sector (roughly corresponding to the PaF1; Figure 2) and Fault Zone 3 in the San Demetrio sector (corresponding to the SGF; Figure 2).

4. Methods and Data Acquisition

We performed an extensive geophysical field survey made up of 86 TDEM soundings coupled with 155 H/V recordings in order to provide an overall subsurface picture of the MAV. We focused our efforts on the accurate location of the buried interface between the basin infill deposits and the top of the Meso-Cenozoic marine substratum (hereinafter top-bedrock). Both TDEM and H/V methods owe their popularity to their relatively easy deployment, cost efficiency, and reliability in detecting the depth of large lithological changes (i.e., resistivity variations and impedance contrast between soft soils and seismic bedrock, respectively), obtaining at the same time significant penetration depths. We then integrated and calibrated our TDEM and H/V measurements with a critically revised set of existing shallow boreholes and other independent geophysical data provided by seismic microzonation studies as well as by the recent literature [*MS-AQ Working Group*, 2010; *Improta et al*., 2012; *Villani et al*., 2015, 2017].

4.1. Time Domain Electromagnetics

TDEM method [*Nabighian and Macnae*, 1991; *Christiansen et al*., 2009] is based on the induction of a time-varying secondary magnetic field (defined with the modulus of magnetic induction vector **B**) associated with an abrupt turnoff of an electrical current flowing in a transmitter loop. The time decay of this secondary magnetic field (dB/dt) recorded by the instrument provides information on the subsurface resistivity, which for near-surface sediments can vary from thousands of Ωm for carbonates or crystalline rocks to a few Ωm for clay and/or saturated alluvium [e.g., *Palacky*, 1987]. The ease of deployment and effectiveness of the TDEM methods results from its ability to reach significant penetration depths despite energizing the subsurface over a relatively small area. In fact, the ratio of penetration depth to loop size for TDEM can be much greater than 1, as opposed to electrical resistivity tomography, where great penetration depths require long electrode arrays [*Revil et al*., 2011; *Pucci et al*., 2016]. Ground TDEM surveys were rarely used in the recent past to map fault zone [e.g., *Bedrosian et al*., 2013] or for depth-to-bedrock investigations over a fault-controlled area [e.g., *Bedrosian et al*., 2012].

In this study, we used a calibrated Geonics digital Protem equipped with both high-frequency 1-D and three-component receiver induction coils, coupled with a transmitter square loop of 50 m and 100 m size [*Sapia et al*., 2015]. We performed TDEM measurements both with central-loop and offset receiver configurations. For the central loop configuration, the receiver induction coil was placed in the center of a square-shaped transmitter loop, while in the offset receiver configuration, the receiver is placed 25 m outside the loop. The input current, gain setting, and number of stacks were determined based on standards from Geonics Ltd. (Rob Harris, personal communication). TDEM soundings were acquired at different repetition frequencies to gather both shallow and deep transient response [*McNeill et al*., 1984]. Repetition frequencies used in this study were high (25 Hz) and medium (6.25 Hz), covering the 80 μs to 28 ms time interval to accurately measure the late time transient amplitudes. Ultrahigh (237.5 Hz) and very high (62.5 Hz) repetition frequencies, covering approximately the 6.7 μs to 800 μs time interval, were only acquired for the calibration check of TDEM data against borehole information (see section 4.4). To choose the optimal loop size and recording time for the TDEM measurements in order to provide a sufficient depth of investigation, we made use of a gravity map, which provided indirect constraints on the top-bedrock surface geometry in the MAV

[*Cesi et al*., 2010]. Furthermore, to check the consistency between TDEM data from different loop sizes and the gravity trend anomalies of *Cesi et al*. [2010], we investigated a few sites by using both 100 m and 50 m loop size. We observed that the long-wavelength gravity anomalies, attributable to deep-seated geological features, were better imaged by using a 100 m loop size, while the 50 m loop size better reproduced the density anomalies attributable to shallower depths to bedrock.

We performed initial electromagnetic noise tests at each site, showing that the signal-noise level was generally high in the studied area. Since the surveys span a large geographic area, we repeated the initial noise tests for each site. This helped us in discarding some unreliable TDEM measurements due to diffuse electromagnetic noise. In addition, data distorted by 2-D or 3-D effects or suffering from issues related to coupling with infrastructures were not considered in the inversion [*Newman et al*., 1986; *Danielsen et al*., 2003].

We processed the data by using the SiTEM software, and the resistivity data were inverted with the SEMDI program [*Effersø et al*., 1999] to obtain 1-D resistivity models of the subsurface. Measured data were inverted by using an iterative least squares inversion algorithm where the system transfer function of the instrument is fully modeled. The estimated model resolution for individual model parameters (layer resistivity, thicknesses, and depth) is presented in relative standard deviation numbers. The depth of investigation (DOI), which represents the maximum depth at which there is sensitivity to the model parameters [*Christiansen and Auken*, 2012], was also computed for each of the output models.

4.2. H/V Analysis of Single-Station Ambient Vibration Surveys

The H/V method applied to single-station ambient vibration recordings has become a widely used technique to retrieve information about the shallow subsurface seismic properties by individual measurements carried out on the Earth's surface. This method requires the acquisition of the ambient vibration wavefield by a three-component seismometer and calculation of the ratio between its horizontal (H) and vertical (V) Fourier spectra, properly averaged on an adequate sample [*Lunedei and Malischewsky*, 2015]. To obtain a robust estimate of the ambient vibration wavefield characteristics, the recording length usually ranges from 30 min to several hours. Processing of the records generally include detrending, windowing, and selection of the time windows to exclude strong transients [*Bard and Site Effects aSsessment using AMbient Excitations Team*, 2005] and smoothing of the calculated spectra [*Konno and Ohmachi*, 1998]. Further, the two horizontal components of the ambient vibration wavefield can be combined in several ways before computation of the H/V ratio [*Albarello and Lunede*, 2013].

It is widely accepted among authors that if a sharp peak is observed in the H/V spectral ratio, the frequency of the H/V peak represents the fundamental resonance frequency (f_0) that can be associated with the depth of the main seismic impedance contrast and the average shear-wave velocity properties above the contrast. In general, where a strong seismic impedance contrast exists at the interface between the bedrock and the sedimentary cover, the H/V method has been successfully used to infer the sedimentary infill thickness inside basins [*Ibs-Von Seht and Wohlenberg*, 1999; *Delgado et al*., 2000; *Uebayashi*, 2003; *Hinzen et al*., 2004; *García-Jerez et al*., 2006; *Bonnefoy-Claudet et al*., 2009; *Langston and Horton*, 2014; *Salloum et al*., 2014]. To this end, under the assumption of 1-D subsurface conditions, namely, considering the subsurface as composed of a stack of homogeneous and isotropic horizontal layers overlying a homogeneous half-space, and provided that a correct estimate of the average shear-wave velocity ($\overline{V}_s$) of the sedimentary cover is available, the thickness of the sedimentary cover (Z) can be roughly estimated by the following relation [*Yamanaka et al*., 1994]:

$$f_0 = \overline{V}_s/4Z$$

However, although the successful applications, the theoretical interpretation of the H/V function is still a matter of debate, mainly related to the unknown ambient vibration wavefield composition [*Lunedei and Malischewsky*, 2015; *Overduin et al*., 2015]. Three main physical interpretations of the H/V have been proposed in the literature [*Piña-Flores et al*., 2016]. The first one directly relates the H/V spectral ratio to the transfer function for vertically incident *SH* waves [*Nakamura*, 1989, 2000], the second one relates the H/V function to the ellipticity of the Rayleigh waves [*Field and Jacob*, 1995; *Horike*, 1996; *Konno and Ohmachi*, 1998; *Lachet and Bard*, 1994; *Nogoshi and Igarashi*, 1971; *Tokimatsu*, 1995; *Wathelet et al*. 2004], and the third one models the H/V on the basis of the diffuse field assumption [*Sánchez-Sesma et al*., 2010, 2011].

The ambient vibration wavefield was recorded by means of 24 bit Reftek130 data loggers (http://www.trimble.com/Infrastructure/Trimble-REF-TEK-130S-01.aspx) coupled to three-component velocimeter (Lennartz LE-3D5s; http://www.lennartz-electronic.de/) with eigenfrequency of 0.2 Hz. We fixed the sampling rate at 250 Hz, using a minimum recording duration of 50 min; however, the majority of measurements had a duration of a few hours. Some measurements, mostly situated in proximity of urban/industrial areas, were discarded after the visual and spectral analysis, because they appeared biased by anthropic activity. We processed the data and computed the H/V curves by using the *Geopsy* code (http://www.geopsy.org).

Reliable shallow velocity profiles were obtained from seismic microzonation studies carried out in the L'Aquila surroundings and in the MAV [*MS-AQ Working Group*, 2010], and mostly by specific studies using surface-wave array analysis [*Di Giulio et al*., 2014]. Typical average values ($\overline{V}_s$) of the shear-wave velocity of the basin infill deposits were estimated in the range of 600–700 m/s. Assuming such values of $\overline{V}_s$ as representative of the average basin infill velocity, the range of possible top-bedrock depths (Z) has been estimated simply as $Z = \overline{V}_s/(4\ f_0)$. However, basins may behave differently than expected from 1-D resonance models [*Roten et al*., 2006; *Michel et al*., 2014], and therefore, there are uncertainties to be considered. The existence of conditions for 1-D or 2-D/3-D amplifications mostly depend on (i) the geometrical shape ratio of the valley, defined as the ratio of the maximum deposit thickness T to the valley half-width L, and (ii) the velocity contrast between sedimentary infill and bedrock [*Bard and Bouchon*, 1985]. Two-dimensional resonance is expected for deep basins generally characterized by a large shape ratio ($T/L > 0.3$) [*Roten et al*., 2006; *Guéguen et al*., 2007; *Le Roux et al*., 2012]. However, the MAV is a shallow alluvial basin where traveling surface waves are dominant in the seismic wavefield, and as discussed below, we obtained a good agreement in terms of top-bedrock depth Z from independent methods (i.e., H/V and TDEM), so we can assume an a posteriori reliability of 1-D seismic resonance of the MAV basin.

4.3. Survey Design

Subsurface geophysical imaging in densely populated areas is not an easy task. It may be hampered by the presence of infrastructures and buried and/or surficial lifelines that pose severe limitations to the survey design, and represent a source of disturbance for electromagnetic and ambient vibration measurements. The selection of suitable measurement sites for TDEM and H/V was carefully planned, considering the location of buried pipelines (water and gas) as well as the paths of major power lines and railways in the area (Figure 3). In fact, whereas TDEM is highly sensitive to the presence of metal fences, pipelines, powerlines, and railroads or even to atmospheric perturbations, H/V can be strongly affected by industrial activities. As a consequence, a portion of the investigated area (Figure 3) has not been covered by TDEM and/or H/V.

Moreover, the complex fault system architecture posed additional requirements of the survey design, especially for TDEM surveys. We took particular attention to keeping enough distance from the known faults in order to avoid possible 3-D effects. However, in some cases we had to disregard TDEM soundings resulting in unreliable 1-D resistivity models [*Goldman et al*., 1984].

The survey campaign was carried out by two crews of three/four operators during about 40 days of acquisition. The main survey design goals were to cover the basin at regular spacing and to have the TDEM and H/V measurement sites co-located. Notwithstanding the logistical difficulties, we achieved a reliable sampling of the area (~75 km^2), obtaining a density of ~3 points/km^2, with an average spacing of ~400 m.

4.4. Calibration of TDEM and H/V Recordings

Prior to our work, the study area was characterized by a few shallow boreholes that reached the pre-Quaternary bedrock in proximity to the Paganica, San Gregorio, and Pianola villages [*MS-AQ Working Group*, 2010; *Giocoli et al*., 2011] (database ISPRA available at http://sgi.isprambiente.it/GMV2/index.html).

We performed an initial calibration of TDEM and ambient vibration recordings near Pianola village, about 2 km to the southeast of L'Aquila downtown (see location of borehole in Figure 3). Here a shallow borehole penetrated Miocene limestones at 96 m depth, and the overlying Quaternary continental sequence was characterized by clayey silt and sandy silt with rare small gravelly layers, most probably related to fluvial and fluvio-lacustrine environments (Figure 4a). The 1-D resistivity models obtained by inversion of TDEM data acquired in close proximity to this borehole show an abrupt increase of resistivity, suggesting the presence of a resistive layer at a depth of 90 m. In addition, assuming for this particular calibration a $\overline{V}_s$ of the basin infill of

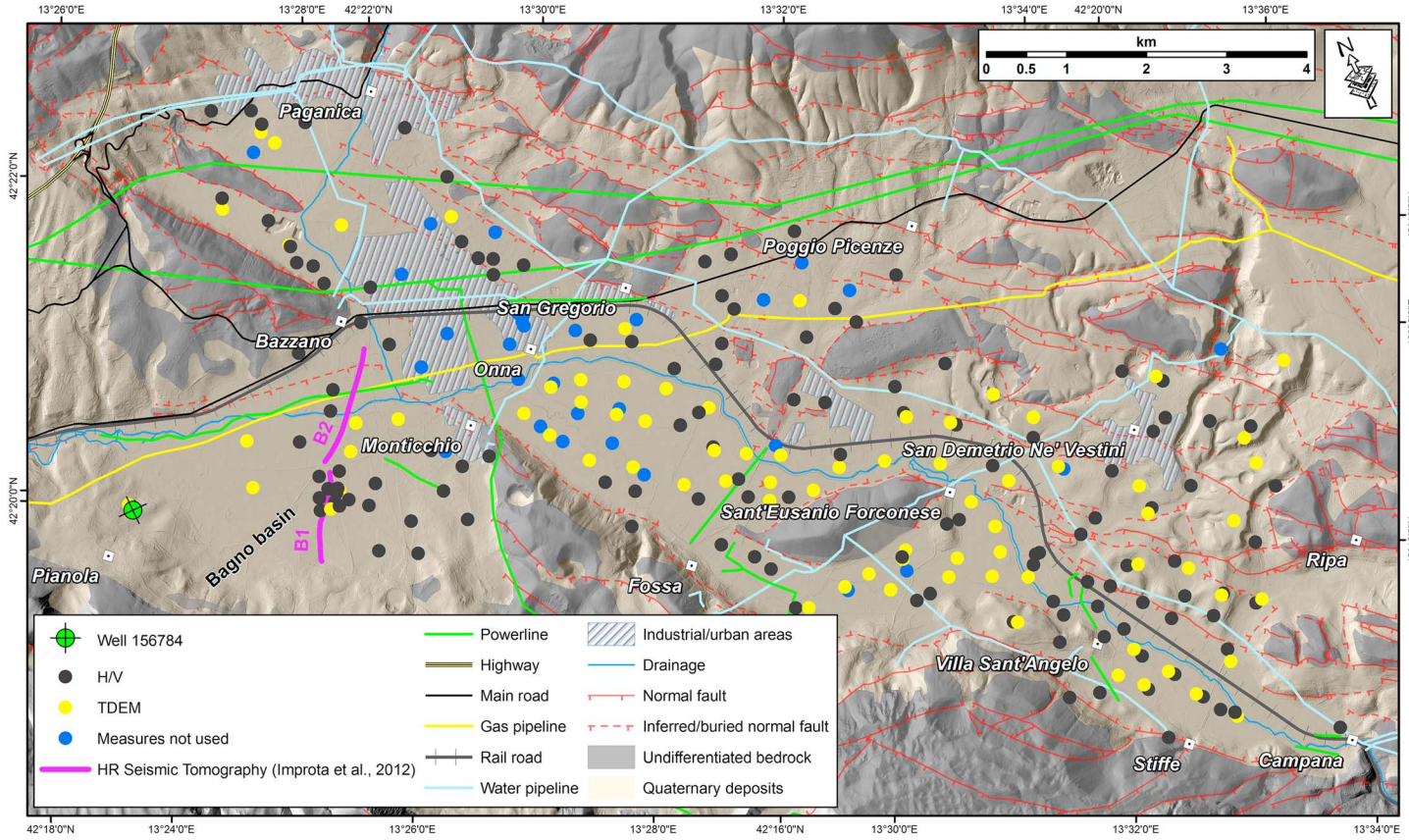

Figure 3. TDEM and H/V measurements in the MAV. The map also shows the main infrastructures and lifelines in the study area. The calibration well is also located with a black and green symbol (http://sgi.isprambiente.it/indagini/scheda_indagine.asp?Codice=156784). Note the rotated north arrow.

550–650 m/s (due to the abundance of silty deposits), the peak frequency resulting from H/V curves ($f_0 = 1.5$ Hz; Figure 4b) is compatible with a top-bedrock at depths ranging between 90 and 110 m. Although TDEM and H/V methods are based on different physical contrasts (electric conductivity and seismic velocity, respectively), the resulting depth of the main interface near the shallow borehole from the two different methods is comparable and in agreement with the observed stratigraphy.

An additional calibration of the two methods was performed in the central portion of the Bagno Basin, where high-resolution V_p tomographic images [*Improta et al.*, 2012] (see also Figures S1 and S2 in the supporting information) indicate a maximum top-bedrock depth of 230–250 m. In this area (corresponding to the seismic profile B1 in Figure 3), seismic stations were placed not only in a single-station H/V configuration but also arranged as three 2-D small seismic arrays. These 2-D arrays were characterized by approximately circular deployments with maximum apertures from 50 to 500 m and were positioned around the 151 m deep borehole LAQUI-CORE drilled in 2013 [*Porreca et al.*, 2016; *Macrì et al.*, 2016]. The aim of the 2-D arrays was to estimate a shear-wave velocity profile from a joint inversion (throughout an improved neighborhood algorithm) of the surface-wave dispersion and H/V curve, similarly to the analysis shown in *Di Giulio et al.* [2014]. Surface-wave methods based on 2-D arrays represent areal surveys because they investigate a large volume of the subsoil medium and are generally able to provide reliable average velocity value ($\overline{V}_s$) in the soft sedimentary cover [see, for example, *Garofalo et al.*, 2016]. The array provided a surface-wave dispersion curve, which was the input of an inversion procedure aimed at deriving a local velocity profile (see Figure S3). We obtained a good fit between field curves and theoretical models assuming for the parameterization of the layered medium, a linear law in the soft layer. The resulting shear-wave velocity models indicated $\overline{V}_s$ in the range of 600–700 m/s for the sedimentary deposits, consistently with the findings of *Di Giulio et al.* [2014] for a similar geological context. Given this convergence, we decided to use a $\overline{V}_s$ in the range of 600–700 m/s for the thickness computation of the soft continental infill within the whole MAV basin.

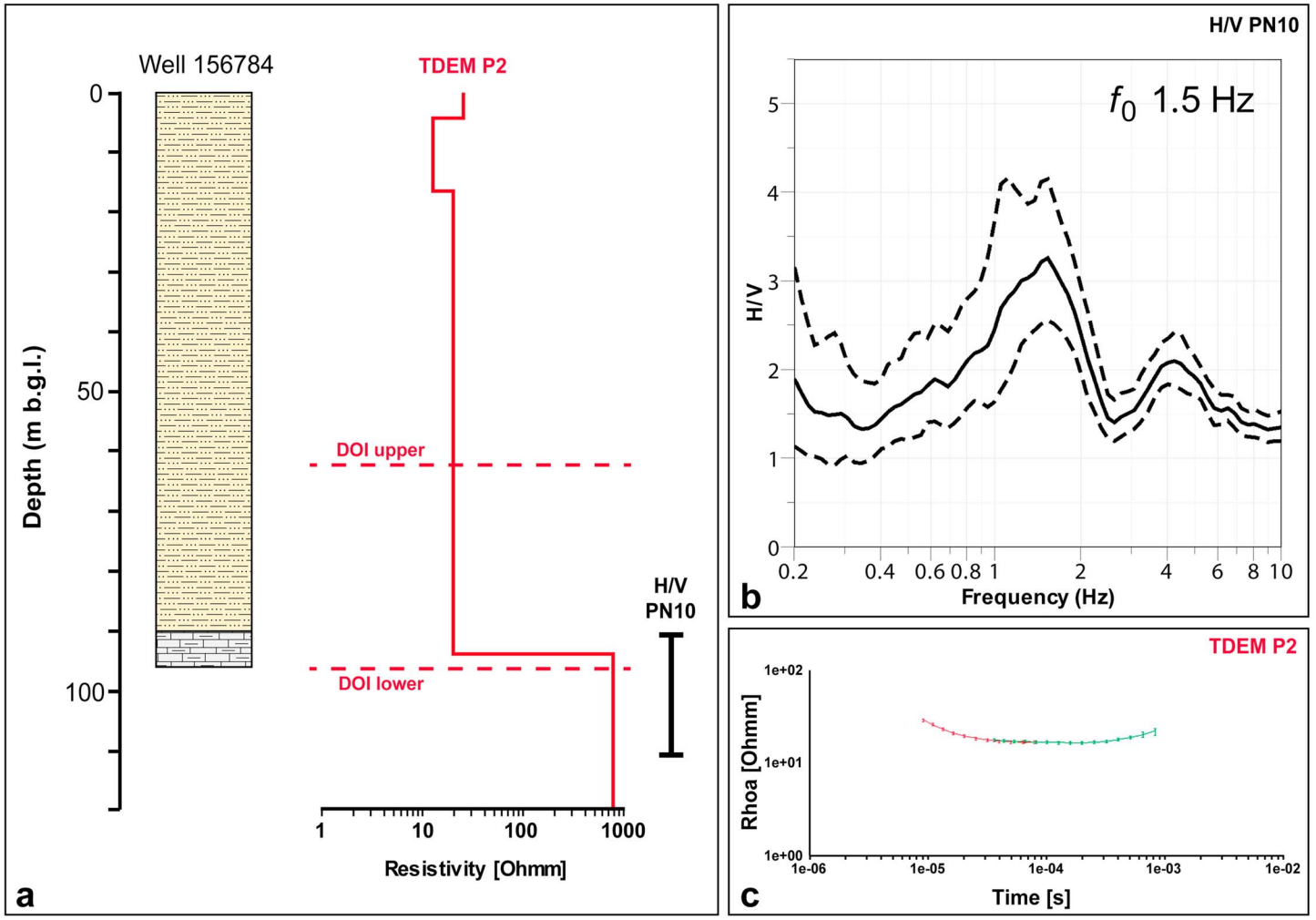

Figure 4. Calibration of TDEM and H/V method. (a) Pianola well log (http://sgi.isprambiente.it/indagini/scheda_indagine.asp?Codice=156784) with TDEM 1-D resistivity models (P2; solid red line) and top-bedrock depth-interval from H/V (PN 10; solid vertical black line). The 96 m depth of the top of the pre-Quaternary carbonate bedrock is detected by both methods. The dashed red lines indicate respectively the upper and lower depths of investigation (DOI) calculated for the TDEM output models [*Christiansen et al*., 2011]. (b) H/V curves computed from the ambient vibration surveys (mean, solid line, and mean ±1 standard deviation, dashed lines). (c) Apparent resistivity curve from the TDEM measurement; the error bars are the observed data for the ultrahigh (red) and very high (green) repetition frequencies, respectively. The forward response (solid line) fits the data within the noise level.

Figure 5 compares the results along profiles B1 and B2 of the 2-D seismic survey performed by *Improta et al*. [2012] with three adjacent TDEM soundings and five H/V measurements. Notably, the depth of the top-bedrock as recovered by both the f_0 trend resulting from H/V curves (Figure 5a) and the TDEM 1-D resistivity models (Figure 5b) is in good agreement (±15 m) with the results of the V_p tomograms, where the top-bedrock is assumed to have a V_p of 3000 m/s (Figure 5c). This example highlights a consistent match between independent estimations of the basin substratum depth and provides an assessment of the uncertainty associated with the measurements.

After this calibration phase, we extended our TDEM and H/V measurements across the entire MAV area (PSDB and Bagno Basin). Figure 6 shows an example of TDEM soundings and H/V measurements performed at three different sites of the MAV characterized by different top-bedrock depths. One-dimensional resistivity models recovered from inversion of TDEM data and depth ranges derived from H/V curves are compared for shallow (Figure 6a), intermediate (Figure 6b), and deep (Figure 6c) top-bedrock depths. These show a consistent match between the estimations of the basin substratum depth within 15%, providing an indication of our depth uncertainty.

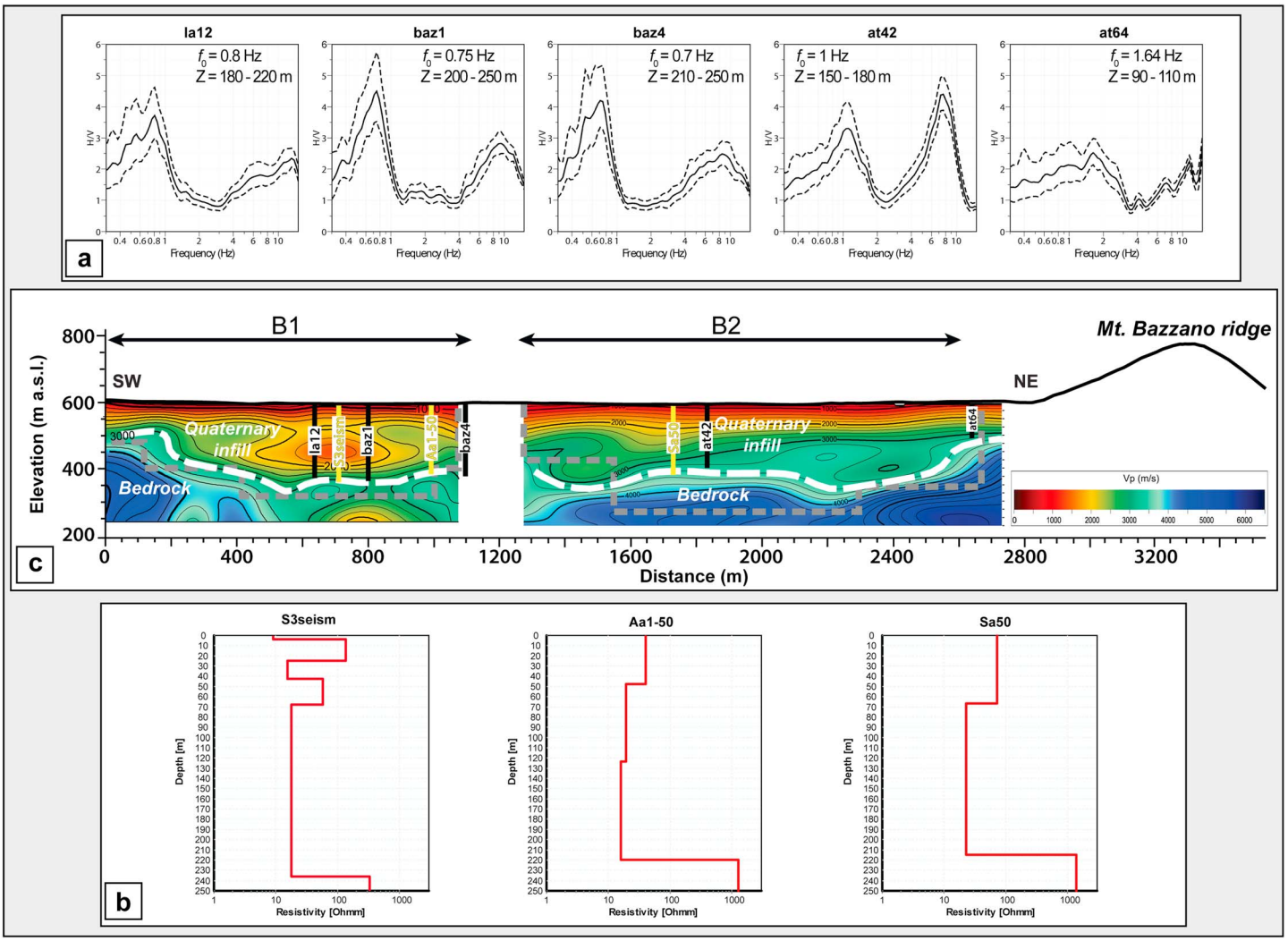

Figure 5. (a) H/V curves computed from ambient vibration surveys. (b) 1-D resistivity models derived from the inversion of TDEM data (solid red lines), projected along the V_P model. (c) V_P tomogram of two high-resolution seismic lines (B1 and B2 in Figure 3) across the Bagno subbasin [modified after *Improta et al.*, 2012] (see Figures S1 and S2 for details) with the location and depth obtained from H/V (black bars) and TDEM (yellow bars) measurements.

4.5. Joint Use of TDEM and H/V Recordings

During the survey, we obtained 77 successful TDEM 1-D resistivity models and 133 successful H/V curves, out of a total of 86 TDEM soundings and 155 H/V recordings (Figure 3 and Table S1). A few H/V recordings were discarded due to technical problems (power failure or cables not working), whereas some H/V data were biased by anthropic activities, especially near the industrial/urban areas (see blue dots in Figure 3). Further, we excluded about 20 additional measurements sites because in those cases TDEM and H/V surveys provided inconsistent results. In the following, we explain the possible causes of this mismatch.

As regard the H/V measurements at these sites, we found that the f_0 peak was not related to the impedance contrast at the top-bedrock - infill interface, but rather to a shallower seismic interface within the continental infill, thus indicating a strong shallow vertical velocity inversion (i.e., shallow stiff conglomerates overlying soft lacustrine clays, as indicated in several shallow boreholes in the area). This happened in the area SE of Monticchio village (Figure 3), where the H/V systematically indicates a shallower stiff interface than the top-bedrock as inferred by TDEM resistivity models. The closest 1-D resistivity models show the presence of the top of a resistive layer attributable to coarse-grained materials at the depth assessed from the H/V records. Furthermore, the a priori geological/geophysical knowledge [*MS-AQ Working Group*, 2010; *Cesi et al.*, 2010] confirms the reliability of the top-bedrock depth as inferred by the 1-D TDEM resistivity

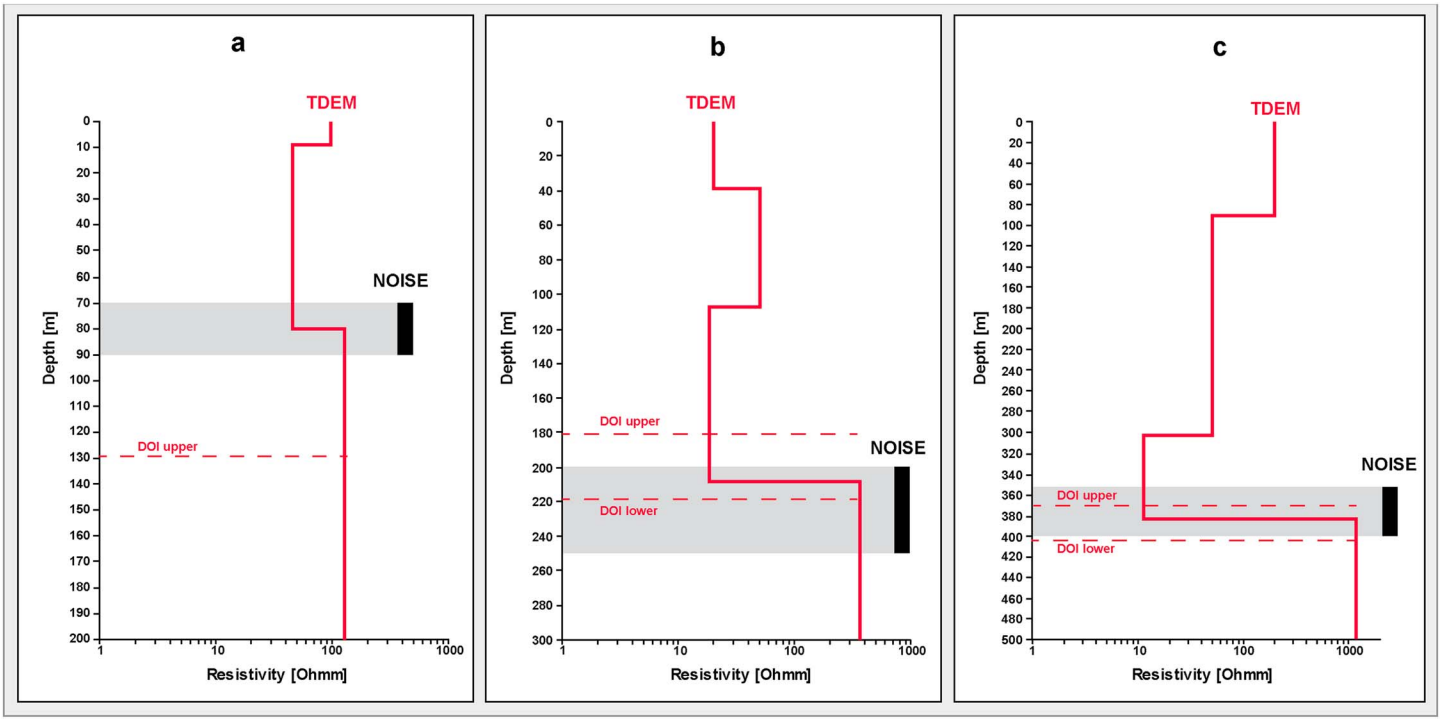

Figure 6. 1-D resistivity models (solid red lines) recovered from inversion of TDEM data and top-bedrock depth-interval (solid vertical black lines) derived from H/V curves for three different top-bedrock depths: (a) shallow (TDEM ID97; H/V ID77), (b) intermediate (TDEM ID109; H/V ID2), and (c) deep (TDEM ID739; H/V ID56) top-bedrock depth obtained from both methods (see Table S1 in the supporting information). The dashed red lines indicate respectively the upper and lower depths of investigation calculated for the TDEM output models [*Christiansen and Auken*, 2012].

models (see also Figure S4). The f_0 and therefore the Z derived from H/V spectral ratio are biased by an uppermost rigid layer (i.e., few meter-thick gravel deposits) overlying soft deposits, which thus masks the seismic resonance of the deep bedrock interface [*Castellaro and Mulargia*, 2009; *Di Giulio et al*., 2016]. In addition, nearly flat H/V curves that would imply outcropping seismic basement are instead found in some areas where stiff conglomerates and/or breccias (thickness of several tens of meters) directly overlie limestones. This is the case in the area between Paganica and Monticchio villages, where the basin is filled with coarse-grained deposits related to alluvial fan accretion, as evidenced by quarry outcrops and shallow boreholes.

Given the complex 3-D geological architecture of the survey area, possible 3-D effects due to the presence of strong lateral resistivity contrast may lead to vanishing of the 1-D assumption for TDEM data modeling. Therefore, we discarded those clearly 3-D affected TDEM data collected in proximity or not sufficiently distant from known 3-D geological features (i.e., faults).

4.6. Data Interpolation

We jointly interpolated the depth to the top-bedrock as recovered from TDEM and H/V analysis and integrated our data set with a set of shallow boreholes and other geophysical data acquired during recent seismic microzonation studies (see Table S1), which we revised in detail. We used a natural neighbor (NN) interpolation technique [*Sibson*, 1981], which performs well with scattered and irregularly spaced data [*Gold*, 1989; *Sambridge et al*., 1995]. The NN interpolation has the advantage of creating an output surface which passes exactly through the input data, without inferring trends or producing peaks, pits, depressions, or ridges that are not already present in the input samples. As primary boundary condition, we imposed the interpolated depth to top-bedrock surface to be zero along the bedrock outcrops within the MAV and along its margins. Additionally, the elevation of the resulting interpolated surface is forced to be lower than the bottom of boreholes that did not penetrate the substratum.

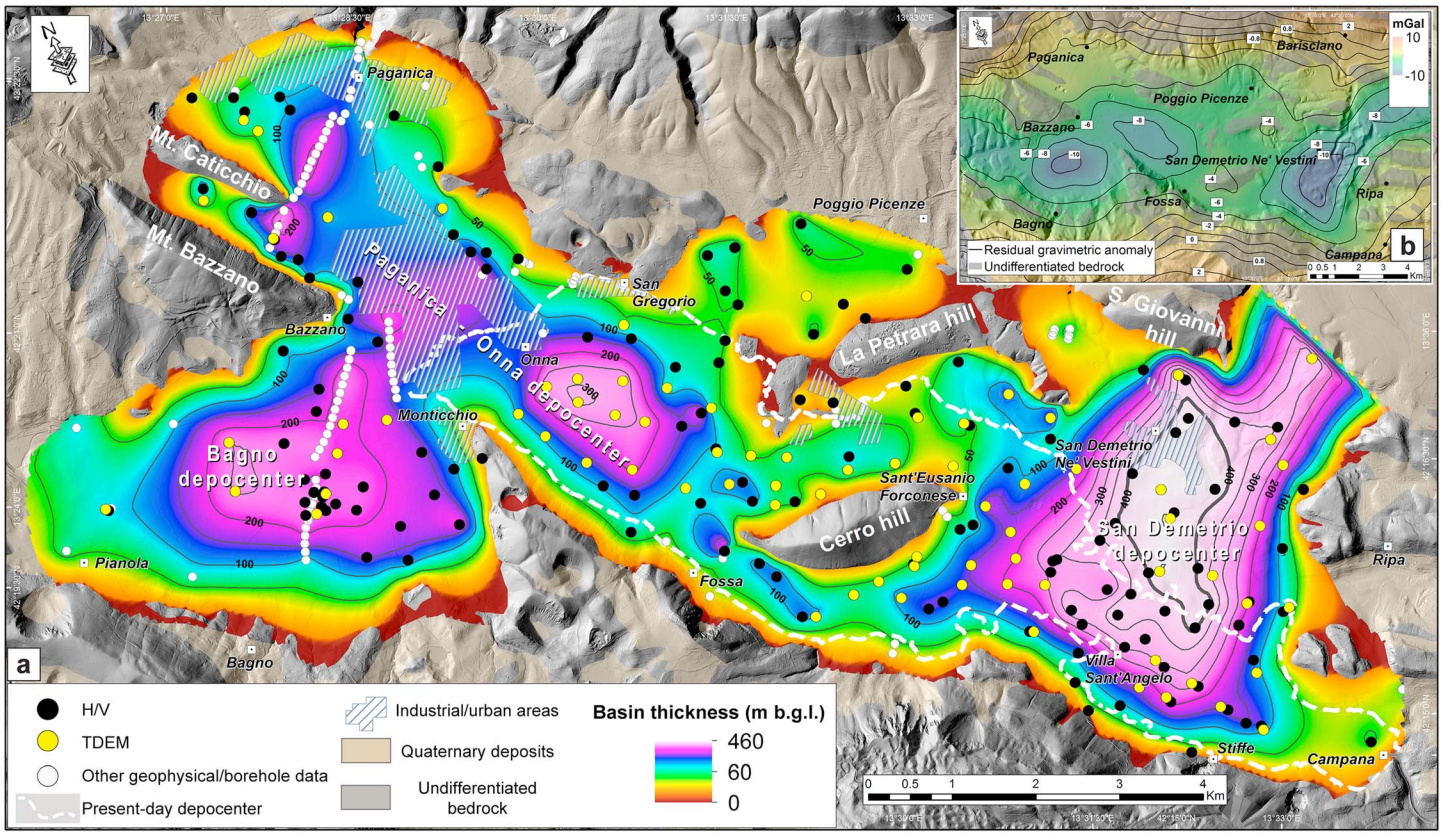

Figure 7. (a) Isopach map of the basin infill (contour interval 50 m), illustrating important thickness variations within the MAV infill. The black and yellow dots locate the H/V and TDEM measurement sites, respectively. The location of the other geophysical and borehole data used in the interpolation is reported, too. The white dashed line encloses the present-day depocenter area (contour line of elevation 583 m asl, defined as the area with average slope $\leq 3°$ enclosing the Aterno River trunk stream). The bold grey thickness contour line encloses the base of the SDD depocenter. (b) Residual gravimetric anomaly map [redrawn after *Cesi et al.*, 2010]. The extent of the inset map is the same of the main map. Note the rotated north arrow.

We selected a grid cell (a.k.a. pixel size) of 70 m for the output maps (Figures 7 and 8). The choice of this grid resolution [*Hengl*, 2006] was related to the number of input depth to top-bedrock points (210 from TDEM and H/V, 101 from shallow boreholes and other geophysical data, and 638 from the edges of bedrock outcrops) and the extent of the investigated area (~75 km^2). This implies that local-scale heterogeneities, related, for example, to minor faulting or erosional features, may not be sufficiently sampled. However, our primary target is the reconstruction of a smooth surface that depicts the first-order topographic features of the top-basement buried under the continental cover.

5. Results

On the basis of the data collected during the survey and of their analysis (described in the previous sections), and by interpolating TDEM, H/V, and stratigraphic data, we were able to map two surfaces: (1) the depth of the top-bedrock with respect to the present-day surface (Figure 7) and (2) the estimated absolute elevation of the top-bedrock (Figure 8). Due to the rough topography of the study area, the quite large range in elevation of measurement points (up to 300 m) has important consequences on the shape of the retrieved top-bedrock surface. Therefore, we describe separately two main output surfaces with different meanings. In the first case (Figure 7), the obtained surface represents an isopach map of the basin infill, irrespective of the absolute elevation of measurement points. In the second case (Figure 8), the interpolated surface represents the actual depth of topography on the basin floor and includes the morphology related to the combined effects of faulting and/or erosional processes acting since the generation of the MAV.

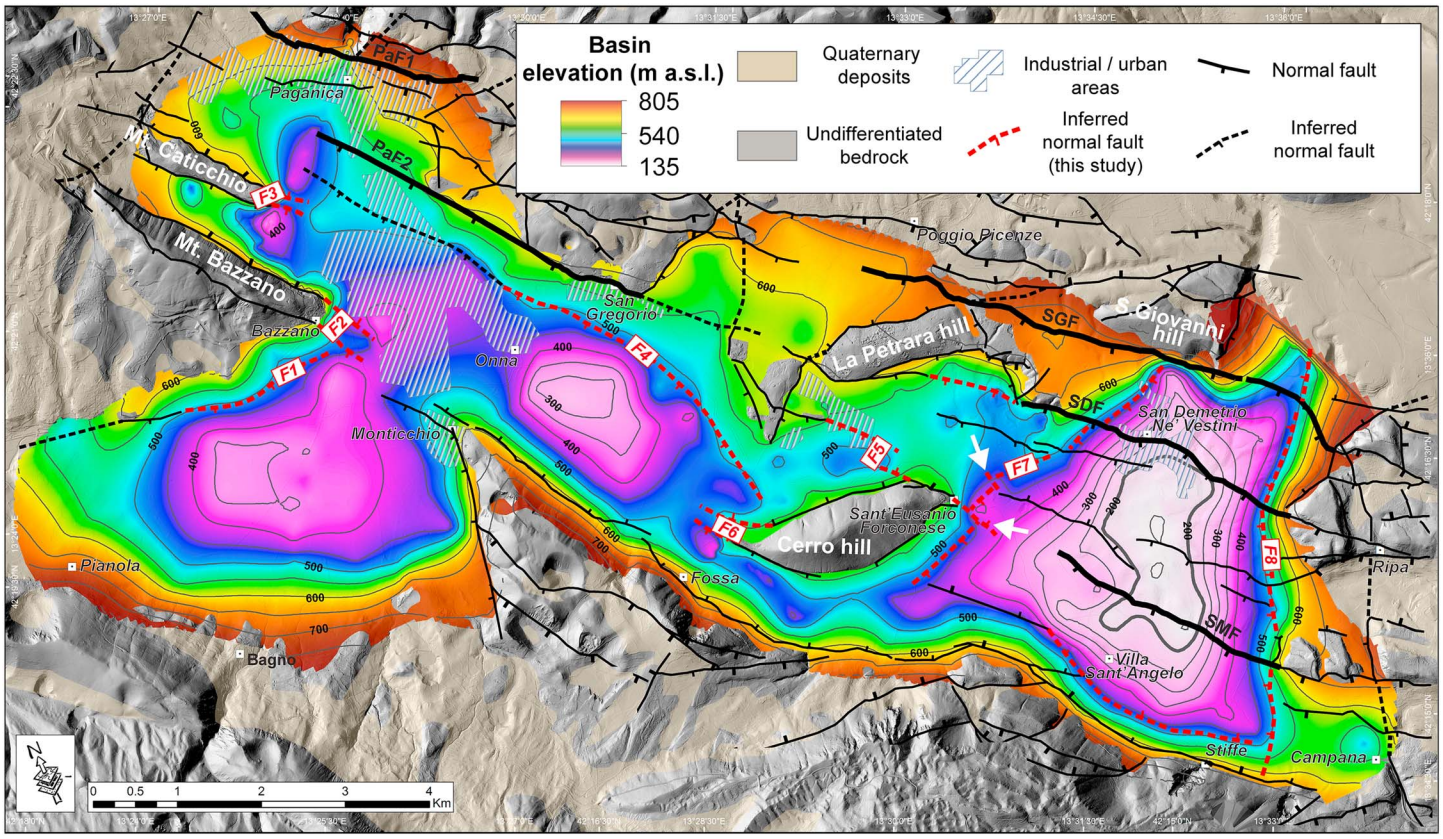

Figure 8. Shape of the continental basin bottom (contour interval 50 m). The basin architecture is compared with the fault system at the surface [modified after *Pucci et al.*, 2014]; inferred buried normal faults are shown in red; major faults of the PSDFS are shown in black bold lines: PaF1, Paganica Fault; PaF2, San Gregorio splay of the Paganica Fault; SGF, San Giovanni Fault; SDF, San Demetrio Fault; SMF, San Mauro Fault. The white arrows indicate the deflection of the elevation contour lines possibly related to the activity of NW-SE trending inferred buried faults. The bold grey elevation contour line encloses the base of the SDD depocenter. Note the rotated north arrow.

5.1. Subsurface Infill Geometry-Quaternary Deposit Thickness

Figure 7 illustrates thickness variations within the MAV infill, pointing out a high complexity of the subsurface, characterized by the presence of three main buried depocenters separated by thresholds: the Bagno (BD), Paganica-Onna (POD), and San Demetrio (SDD) depocenters.

The BD shows an E-W elongated shape and a nearly flat bottom; the maximum thickness of the infill is ~220–240 m. A low-gradient buried saddle between Monticchio and Bazzano villages separates the BD from the POD area.

The POD area (between the villages of Bazzano, Monticchio, Fossa, San Gregorio, and Paganica) shows the inferred sedimentary thickness deepening southward and reaching a maximum value of ~300 m south of Onna village. Here the depocenter presents a roughly NW-SE oriented rectangular shape, which is constrained by a large amount of data. Another depocenter, with an inferred maximum thickness of ~250 m, is located in the northern sector of the basin between Paganica village and the Caticchio and Bazzano ridges; however, due to the lack of data in coincidence within the large industrial area, here the geometry of the top-bedrock is poorly constrained.

The deepest depocenter (SDD) is located at the southern end of the MAV (between San Demetrio ne' Vestini, Villa Sant'Angelo, and Sant'Eusanio Forconese villages). The SDD is characterized by a roughly trapezoidal shape, a nearly flat base (see bold grey contour line in Figure 7) and by a maximum thickness exceeding 450 m. An outstanding feature is the rectilinear and sharp (~40%) thickness gradient of the NNE-SSW oriented, southeastern side of the MAV.

It is noteworthy that in the central part of the MAV the isopach map indicates a reduced thickness of the basin infill deposits around the outcropping bedrock ridges of Cerro and La Petrara hills (greenish and yellowish areas in Figure 7). This ~ENE-WSW trending, partly buried structural high represents a threshold between the POD and SDD areas.

5.2. Subsurface Geometry-Basin Bottom Topography

Figure 8 shows the actual deep topography of the MAV Basin floor under the continental Quaternary infill. The MAV bottom is characterized by a complex top-bedrock morphology and confirms the three main sectors with different geometries also observed in Figure 7: (1) the BD, (2) the POD, and (3) the SDD.

The buried topography of the MAV floor is characterized by narrow belts of pronounced elevation gradients. We interpreted these features as a possible evidence of the presence of buried tectonic structures (red dashed lines in Figure 8) when they are characterized by high ($>$40%) or relatively high ($>$20%) elevation gradients or when they have a linear extension $>$1 km; it is noteworthy that in most of the cases these are the prolongation of tectonic structures visible at the surface [*Pucci et al*., 2014, 2015].

The BD is characterized by a high-elevation gradient on its eastern side, compatible with the presence of the tectonic structure mapped at the surface. Relatively high-elevation gradients define the northern side of the BD; here we hypothesize the presence of a buried fault as the prolongation of a tectonic structure recognized at the surface (F1 in Figure 8).

As for the POD, the high and relatively high-elevation gradients visible on its southwestern and northeastern sides, respectively, may be evidence of a structural control exerted by the NW-SE striking PSDFS. In particular, we hypothesize the presence of an ~4.5 km long buried normal fault (F4 in Figure 8), which may represent an additional splay in the hanging wall of PaF2 (see also Figure 2). Interestingly, F4 is the southeastern extension of a shallow blind fault mapped in *Boncio et al*. [2010] and in *Pucci et al*. [2015] in the hanging wall of PaF2, based on the occurrence of 2009 coseismic surface cracks. The location, geometry, and throw of this fault have been recently assessed through high-resolution refraction tomography by *Villani et al*. [2017]. Moreover, the northwestern sector of the POD appears to be dissected by a possible subsurface extension of the normal faults bordering the Mount Bazzano and Mount Caticchio ridges at the surface (F2 and F3, respectively, in Figure 8).

The trapezoidal shape of the deepest depocenter (SDD), as well, is not completely coherent with the NW trending, Quaternary normal faults of the PSDFS. The most obvious features of the SDD are the high rectilinear elevation gradients visible on its northwestern and southeastern sides (F7 and F8, respectively, in Figure 8). In our interpretation, the southeastern side of the SDD may be controlled by a NNE-SSW oriented buried tectonic structure (F8 in Figure 8), which noteworthy has a similar strike to the normal faults outcropping in the Ripa village area (see also Figure 2). Here the long-term activity of its southwestern section, by down-throwing the WNW fault block down, resulted in the generation of a morphologic threshold, where the basin infill thins out to 50 m, similarly to that exposed at an elevation of ~550 m asl near Campana village. Notably, at the northwestern side of the SDD, the ~ENE-WSW oriented inferred normal fault (F7 in Figure 8) appears to be dissected by the NW-SE normal faults of the PSDFS. In addition, a sharp elevation gradient is visible to the NE of the San Demetrio ne' Vestini village, in coincidence with the subsurface projection of the San Giovanni fault (SGF).

6. Discussion

As previously discussed, only a few studies have investigated the shallow subsurface of the MAV and its relations with the PSDFS. Information on the subsurface geometry of the MAV is accurate but limited to local existing 2-D high-resolution seismic and ERT surveys. Notwithstanding the uneven distribution of data points and the resulting interpolation surfaces may introduce some uncertainty in the geologic interpretation, this work provides the most complete 3-D picture of the MAV at depth and allows us to speculate on the subsurface geometry and on the relation between the structural setting and the Quaternary basin evolution.

6.1. Subsurface Geometry and Quaternary Infill of the Basin

Our results highlight a complex buried structure of the MAV Basin, characterized by several topographic highs and lows representing thresholds and depocenters, respectively (Figures 7 and 8). Thickness

variations within the MAV infill show a southward thickening of the Quaternary sequences (Figure 7). As a whole, the MAV deepens lengthwise from ~200–300 m in the northern area to a maximum of ~450 m to the south. This thickening is in agreement with the observed southward thickening of the outcropping Quaternary sequence [*Pucci et al*., 2015] and is confirmed by 2-D ERT transects recently performed in the area [*Pucci et al*., 2016] (see Figure 1 for location), which highlight the presence of a deepest buried depocenter located at the southern end of the MAV (SDD).

Furthermore, the overall subsurface basin geometry is congruent with the residual gravimetric anomaly map of *Cesi et al*. [2010] (Figure 7b) produced independently in the same area. In fact, the areas with maximum infill thickness match well the negative Bouguer anomalies.

6.2. Relationship Between Structural Setting and Quaternary Basin Evolution

Taking into account the capabilities and limitations of the subsurface model depicted so far, we can speculate on the possible long-term evolution of the MAV Basin and of the basin-bounding PSDFS. The 70 m pixel size of the modeled surface representing the basin bottom of the MAV allows the depiction of the first-order topographic features of the top basement under the continental cover, while local-scale heterogeneities and details related to minor faulting and/or erosional/depositional features may not be sufficiently sampled.

The MAV is tectonically controlled by normal faults that are part of both the NW-SE striking PSDFS and of the ~ENE and NNE trending extensional fault systems. The MAV experienced considerable modifications in its architecture over time, which resulted in the generation of landforms that today are totally or partially buried below the basin infill. Several factors suggest a predominant structural control on the origin and evolution of the MAV, particularly in the PSDB area, ruling out a predominant role of fluvial incision in the shaping of the valley: (1) the prominent and localized elevation gradients, which may be evidence of buried faults (Figure 8), compatible with the fault arrangement as recognized at the surface [*Pucci et al*., 2014, 2015]; (2) the presence of different buried depocenters separated by thresholds; and (3) the quite flat bottom of the main depocenters (Figure 8). The existence of several tectonic features that produced buried cumulative landforms and controlled the development of depocenter acting as sedimentary traps is also in agreement with the recent findings of 2-D ERT [*Pucci et al*., 2016] and high-resolution seismic investigations in the area [*Villani et al*., 2017].

The shape of the BD is possibly related to the activity of the NNE and WNW trending extensional fault systems (see section 2), rather than having originated as response to NW-SE faulting. Moreover, the buried threshold between the villages of Bazzano and Monticchio (see section 5.1) may suggest a structural continuity of the Mount Bazzano-Fossa-Stiffe ridge (Figure 8). In this perspective, the BD could represent a separate basin, structurally disconnected from the POD.

As regard the POD, based on the spatial distribution of measurement points, the high and relatively high-elevation gradients paralleling some of the NW-SE oriented splays of the PaF (e.g., F4 in Figure 8) and its antithetic splays are well constrained. However, the lack of data points within the industrial area east of Bazzano village leads to a speculative connection between the Paganica and Onna sectors. As a consequence, the overall ~NW-SE elongated geometry of the POD could be an artefact of the model, and we cannot exclude the disruption of the POD bottom by differently oriented (e.g., ~ENE-WSW) faults.

The geometry of the SDD area is well defined due the high density of data points and is characterized by an evident discrepancy between the trapezoidal shape of the old buried depocenter (see bold grey contour line enclosing the base of the depocenter in Figure 7) and the position and shape of the present-day one (Figure 7). The present-day landscape in the SDD area, as well as the distribution of the Holocene deposition (Figure 2), hints at the recent tectonic control being exerted by the NW-SE oriented PSDFS. This may suggest a polyphase evolution of the SDD: the ~ENE and NNE trending extensional fault systems (e.g., F7 and F8 in Figure 8) played an important role during the early stage of basin development (Pliocene?-early Pleistocene), while in a later phase the activity of the NW-SE oriented PSDFS became predominant. An additional clue for this interpretation is given by the overall regular pattern of both the isopachs (Figure 7) and the elevation contour lines (Figure 8), which only in a few places display small deflections. We interpret these deflections as due to the NW-SE trending normal faults crosscutting older structures (e.g., faults F5 cutting fault F7; white arrows in Figure 8). Therefore, the unexpected trapezoidal shape of the SDD may be the result of the "interference" of differently oriented fault systems in this sector.

Moreover, the active depocenter located in the hanging wall area of the San Mauro Fault (SMF in Figure 8), when compared with the position of the buried and older depocenter (bold grey contour lines enclosing the base of the depocenter in Figures 7 and 8), suggests a southwestward depocenter migration over time, possibly related to the activation of progressively younger NW trending faults from the NE (SGF) to the SW (SDF and SMF; Figure 8). This spatiotemporal evolution is also confirmed by the distribution of the post-early Pleistocene deposit infill, marked by a strong top-sequence unconformity: *Pucci et al*. [2014], for instance, report the displacement and uplift of early Pleistocene alluvial sequences by the activity of NW trending faults, and the progradation to the SW of the middle-late Pleistocene alluvial successions developed as a consequence of the hydrographic network response to the fault-related base-level drop.

The geometry of the SDD and POD at depth discussed so far suggests that they possibly originated as separate basins controlled by the activity of previously isolated and differently oriented fault systems. Notably, also the separation between the POD and the SDD arises from the bedrock high outcropping in the area between Cerro and La Petrara hills (Figure 8) that is controlled by ~ENE trending faults [*Pucci et al*., 2014, 2015] (Figure 8). Hence, the activity of ~ENE and NNE trending extensional faults, inherited from the pre-Quaternary compressional phase (see section 2), contributed to create a complex "horst and graben" basin bottom architecture.

Furthermore, we hypothesize small NW trending normal faults (i.e., F5 and F6 in Figure 8), which are the prolongation of tectonic structures mapped at the surface and disrupt the partly buried structural high separating the POD from the SDD, suggesting the breaching of the inherited basin bottom morphology. We interpret this breaching as a possible evidence of a later inception of the activity of the NW trending faults, which are now overprinting and crosscutting the ~ENE and NNE trending extensional faults. The above mentioned evidence, together with the shift of the fault-related locus of deformation from the NE to the SW in the San Demetrio ne' Vestini sector, may suggest a later linkage of the PaF (and its hanging wall splays, including F4) with the SDF/SMF. This hypothesis may also explain the subtle fault-related morphological expression observed at the surface in the central sector of the PSDFS (between San Gregorio and Sant'Eusanio Forconese villages; Figure 8), as also reported by *Civico et al*. [2015].

In summary, the MAV Basin has experienced considerable modifications in its architecture over time, and its present overall geometry evidences a tectonic control by normal faults pertaining both to the NW-SE striking PSDFS and older ~ENE and NNE trending extensional fault systems. The overall buried shape of the PSDB and the crosscutting relationships between the different fault systems suggest a recent and present-day predominant tectonic control by the NW-SE oriented PSDFS.

6.3. Seismotectonic Implications and Contribution to Seismic Hazard

At a basin-wide scale, our subsurface model depicts a complex subsurface architecture of the MAV, characterized by several buried faults. However, it is noteworthy that the fault splays suggested by our 3-D model are closely spaced (1 km or less) and may join at quite shallow depth, becoming a unique quasi-planar fault (the 6 April 2009 earthquake source) from a few kilometers down to seismogenic depths (9–11 km), as also suggested by high-precision aftershock relocations [*Chiaraluce et al*., 2011; *Chiaraluce*, 2012; *Valoroso et al*., 2013].

Although some internal complexities exist, the crosscutting relationships between the different fault systems, the breaching of the inherited basin bottom morphology, and the shift of the depocenter in the SDD area (see section 6.2) point to there possibly being an individual SW dipping normal fault system extending from Paganica to south of San Demetrio ne' Vestini (Figure 8). Our results are compatible with the 2009 main shock causative fault at depth as previously modeled by seismologic-geodetic data (see a review in *Vannoli et al*. [2012] and in *Chiaraluce* [2012]).

The reconstruction of the 3-D architecture of the PSDB at depth also allowed us to provide additional constraints on the location of the PSDFS boundaries, which are of critical relevance for defining the actual length of the fault and thus for estimating the maximum expected magnitude (M_{max}) of the earthquake it can generate. The southeastern margin of the PSDB is characterized by a high topographic gradient, compatible with the presence of a ~5 km long NNE-SSW trending tectonic structure (F8 in Figure 8 - see also section 5.2). This structure appears to have played an important role in the initial stage of basin evolution, allowing the southern portion of the basin to deepen well below (~150 m asl) the present-day basin

morphologic threshold, located near the Campana village (~550 m asl; Figure 8). Furthermore, this tectonic structure may act as a permanent boundary, controlling the extent to the SE of both the buried (bold grey contour lines enclosing the base of the depocenter in Figures 7 and 8) and the present-day basins (Figure 7). Interestingly, the position of this boundary roughly coincides with the southeastern tip of the PSDFS and with the northwestern tip of the MAFS (Figure 2), as derived by the decrease of their morphological throws [*Civico et al*., 2015]. In this perspective, the NNE-SSW trending major buried tectonic structure (F8 in Figure 8) could act as a permanent boundary for the long-term evolution of the PSDFS. Moreover, it could have played a role as a boundary for the 2009 earthquake fault rupture, as evidenced by the abrupt termination of the relocated seismicity [*Chiaraluce et al*., 2011].

An additional clue for this is given by the pattern of shear-wave crustal anisotropy observed by *Baccheschi et al*. [2016] in a wide area of the central Apennines enclosing the epicentral sector of the 2009 L'Aquila earthquake. These authors found that the mean fast polarization directions are generally parallel to the maximum horizontal stress active in the region as well as to the strike of the major Quaternary normal faults, whereas in the southeastern portion of the PSDFS a significant azimuthal change occurs: this is particularly clear at the FAGN seismic station (less than 1 km southeast of Ripa village; Figure 8), where they observed NE-SW oriented mean fast polarization directions, thus almost parallel to the NNE-SSW trending major buried tectonic structure (F8 in Figure 8) suggested by our 3-D model.

Given the position of this southeastern boundary, and taking into account the location of the northern boundary of the PSDFS south of the Collebrincioni village [*Civico et al*., 2015] (see Figure 2), the resulting length of the PSDFS is approximately 19 km. The alignment given by the linkage of the PaF and the SDF-SMF could represent the most active surface trace of the PSDFS, in agreement with previous findings of *Giaccio et al*. [2012], *Blumetti et al*. [2013], and *Civico et al*. [2015] on the basis of geologic and morphotectonic considerations. Our interpretation implies that the PSDFS can also rupture the whole 19 km long structure at the surface, allowing earthquakes with $M > 6.5$, as suggested by currently accepted empirical scaling laws between fault length and magnitude [*Wells and Coppersmith*, 1994], whereas during the 2009 main shock only a small section of the fault ruptured. This could explain the record of some Holocene paleo-earthquakes possibly larger than those that occurred during the 2009 L'Aquila earthquake [*Cinti et al*., 2011].

If we consider the top-bedrock surface (Figure 8) as the basal unconformity of the Plio-Quaternary succession filling the basin, it could be used as a geological marker to infer long-term throw rates of the PSDFS, provided a correlative surface at the fault system footwall is available. Taking into account morphologic throw profiles by *Civico et al*. [2015], with our model we estimate throws of nearly 1000 m in the San Gregorio sector and ~800 m in the San Demetrio ne' Vestini sector. However, due to the lack of chronological constraints on the age of the lowermost sediments, caution should be paid. *Pucci et al*. [2016] estimated throw rates in the 0.2–0.3 mm/yr range, and *Villani et al*. [2017] found similar values in the Paganica sector, assuming extension started at the beginning of Pleistocene (2.59 Ma). Similarly, if we consider a late Pliocene-early Pleistocene age of the basal deposits, we get long-term throw rates of 0.30–0.38 mm/yr. Prudence is also needed when calculating deformation across the PSDF: considering the crosscutting relationships between the two different fault systems participating in the shaping of the MAV Basin, these values have to be considered as maximum throw rates of the overall PSDFS. Additional comprehensive work will be devoted to this topic.

The results of this work are also important for scenario-based seismic hazard analyses at basin-wide scale, because wave reverberation and local ground-motion amplification are primarily controlled by sharp seismic velocity contrasts and geometric complexities in the buried bedrock topography. Basin effects have been clearly recognized in literature, being the topic of many experimental and numerical studies on seismic wave propagation [*Pitarka et al*., 1998; *Graves et al*., 1998; *Semblat et al*., 2005; *Bindi et al*., 2009; *Chaljub et al*., 2010; *Boué et al*., 2016; among many others]. These studies evidenced the fundamental role of the buried geometry in influencing the spatial variability of ground motion within sedimentary basins.

7. Conclusions

The joint use of TDEM soundings and single-station ambient vibration surveys has provided the so far most complete 3-D model of the Middle Aterno Valley (MAV) at depth, in the area of the 2009 L'Aquila earthquake. By reconstructing the buried interface between the infill deposits and the top of the pre-Quaternary

substratum, this work shows a basin-size picture of the subsurface setting of the MAV, which has allowed us to define the subsurface geometry and the relationships between the structural setting and the Quaternary basin evolution.

The recovered buried bedrock morphology shows a complex subsurface architecture of the MAV, characterized by topographic highs and lows, representing thresholds and depocenters. We recognized three main depocenters, characterized by different buried geometries and infill thicknesses. As a whole, thickness variations of the Quaternary deposits show that the MAV deepens lengthwise from ~200–300 m in the northern area to a maximum of more than 450 m to the southeast.

We identified several buried tectonic structures compatible with the fault arrangement as recognized at the surface. At a basin-wide scale, our subsurface model highlights that the MAV experienced considerable modifications in its architecture over time, and its overall geometry evidenced a tectonic control by normal faults that are part of both the NW-SE striking PSDFS and of older ~ENE and NNE trending extensional fault systems. The overall buried shape of the PSDB and the crosscutting relationships between the different fault systems suggest a recent and present-day predominant tectonic control by the NW-SE oriented Paganica-San Demetrio Fault System (PSDFS).

We gained insights into the long-term PSDFS behavior and evolution, evidencing a southwestward depocenter migration over time in the SDD area, possibly related to a migration of fault activity from the SGF (to the NE) to the San Demetrio and San Mauro faults (to the SW; Figure 8). In addition, the geometry of the SDD and POD at depth suggests that they possibly originated as separate basins controlled by the activity of previously isolated and differently oriented fault systems.

Furthermore, we postulate that the present-day arrangement of the PSDFS is the result of the linkage of two previously isolated fault segments, which would imply the presence of a single SW dipping normal fault extending from Paganica to south of San Demetrio ne' Vestini. We have provided additional constraints on the location of the southeastern boundary of the PSDFS, defining an overall length of the fault system of ~19 km. Our interpretation implies that the PSDFS could potentially rupture the whole 19 km long structure at the surface, allowing earthquakes larger than *M* 6.5, besides rupturing only small sections, as occurred in 2009.

This study clearly emphasizes the benefit of combining two different easily deployable, relatively inexpensive geophysical methods in reconstructing the 3-D geometry of a tectonically controlled basin at depth. Given that TDEM and ambient vibration surveys are based on different physical contrasts and are thus sensitive to different types of noise, their joint use allowed us to overcome some of the limitation commonly found in urban/developed areas. TDEM surveys are able to depict resistivity interface usually at larger depth with respect to ERT surveys but can be limited by 3-D structures and electromagnetic noise. Ambient vibration surveys work fine in the presence of a strong impedance seismic contrast (>3), but can be biased by anthropic activities, and the recognition of a resonance frequency is difficult in presence of a not normally dispersive site (i.e., stiff layers overlaid to soft layers). In addition, the combined use of TDEM soundings and single-station ambient vibration surveys, integrated with geological information, allowed us to cross-check for consistency between the two methodologies. As a whole, we obtained a consistent match between independent estimations of the basin substratum depth within an ~15% uncertainty range. The outlined multidisciplinary approach is novel for active tectonic areas, and it could represent an important reference for the development of such studies in similar geological settings.

Acknowledgments

This work has been founded by the FIRB-Abruzzo project, "High-resolution analyses for assessing the seismic hazard and risk of the areas affected by the 6 April 2009 earthquake" (http://progettoabruzzo.rm.ingv.it/en; funding codes: RBAP10ZC8K_005, RBAP10ZC8K_003, and RBAP10ZC8K_007). We are grateful to the Editor and Associated Editor for the editorial handling. Ken McCaffrey, Richard Collier, and one anonymous reviewer provided thoughtful comments that greatly improved the early version of this manuscript. We are also grateful to Rob Harris (Geonics Ltd.), Antonio Menghini, and Andrea Viezzoli (Aarhus Geophysics Aps) for their technical support in TDEM data acquisition and data modeling and to Fernando Ferri for the useful discussions on the residual gravimetric anomaly map. We thank C.A. Brunori, P.M. De Martini, G. Milana, S. Orefice, S. Pinzi, and T. Ricci for their support in the field. The data used can be found in the supporting information and in the cited references.

References

Adamoli, L. (1992), Evidenze di tettonica d'inversione nell'area Corno Grande-Corno Piccolo (Gran Sasso d'Italia), *Boll. Soc. Geol. Ital.*, *111*, 53–66.

Aki, K. (1988), Local site effect on ground motion. In: J.L. Von Thun (Editor), Earthquake Engineering and Soil Dynamics. It: Recent Advances in Ground-Motion Evaluation, *Am. Sot. Civil Eng. Geotech. Spec. Publ.*, *20*, 103–155.

Albarello, D., and E. Lunedei (2013), Combining horizontal ambient vibration components for H/V spectral ratio estimates, *Geophys. J. Int.*, *194*, 936–951, doi:10.1093/gji/ggt130.

Baccheschi, P., M. Pastori, L. Margheriti, and D. Piccinini (2016), Shear wave splitting of the 2009 L'Aquila seismic sequence: Fluid saturated microcracks and crustal fractures in the Abruzzi region (central Apennines, Italy), *Geophys. J. Int.*, *204*(3), 1531–1549, doi:10.1093/gji/ggv536.

Bagh, S., L. Chiaraluce, P. De Gori, M. Moretti, A. Govoni, C. Chiarabba, P. Di Bartolomeo, and M. Romanelli (2007), Background seismicity in the Central Apennines of Italy: The Abruzzo region case study, *Tectonophysics*, *444*, 80–92, doi:10.1016/j.tecto.2007.08.009.

Bagnaia, R., A. D'Epifanio, and S. Sylos Labini (1992), Aquila and sub-aequan basins: An example of Quaternary evolution in central Apennines, Italy, *Quat. Nova*, *II*, 187–209.

Balasco, M., et al. (2011), Deep geophysical electromagnetic section across the middle Aterno Valley (central Italy): Preliminary results after the April 6, 2009 L'Aquila earthquake, *Boll. Geofis. Teor. Appl.*, *52*, 443–455, doi:10.4430/bgta0028.

Bard, P. Y., and M. Bouchon (1980), The seismic response of sediment-filled valleys. Part 2. The case of incident P and SV waves, *Bull. Seismol. Soc. Am.*, *70*(5), 1921–1941.

Bard, P. Y., and M. Bouchon (1985), The two-dimensional resonance of sediment-filled valleys, *Bull. Seismol. Soc. Am.*, *75*(2), 519–541.

Bard, P. Y., and Site Effects aSsessment using AMbient Excitations Team (2005), Report D23.12, Guidelines for the implementation of the H/V spectral ratio technique on ambient vibrations measurements, processing and interpretation, in European Commission: Research general directorate, Project No. EVG1-CT-2000-00026, SESAME, 62 pp. [Available at http://sesame.geopsy.org/SES_Reports.htm (last accessed November 2016).]

Bedrosian, P. A., B. L. Burton, M. H. Powers, B. J. Minsley, J. D. Phillips, and L. E. Hunter (2012), Geophysical investigations of geology and structure at the Martis Creek Dam, Truckee, California, *J. Appl. Geophys.*, *77*, 7–20.

Bedrosian, P. A., M. K. Burgess, and T. Nishikawa (2013), Faulting and groundwater in a desert environment: Constraining hydrogeology using time-domain electromagnetic data, *Near Surf. Geophys.*, *11*(5), 545–555, doi:10.3997/1873-0604.2013043.

Bertini, T., and C. Bosi (1993), La tettonica quaternaria della conca di Fossa (L'Aquila), *Il Quaternario*, *6*, 293–314.

Bindi, D., S. Parolai, F. Cara, G. Di Giulio, G. Ferretti, L. Luzi, G. Monachesi, F. Pacor, and A. Rovelli (2009), Site amplification observed in the Gubbio basin, Central Italy: Hints for lateral propagation effects, *Bull. Seismol. Soc. Am.*, *99*(2A), 741–760.

Blumetti, A. M., L. Guerrieri, and E. Vittori (2013), The primary role of the Paganica-San Demetrio fault system in the seismic landscape of the Middle Aterno Valley basin (Central Apennines), *Quat. Int.*, *288*, 183–194.

Boncio, P., G. Lavecchia, and B. Pace (2004), Defining a model of 3D seismogenic sources for seismic hazard Assessment applications: The case of central Apennines (Italy), *J. Seismol.*, *8*(3), 407–425, doi:10.1023/B:JOSE.0000038449.78801.05.

Boncio, P., A. Pizzi, F. Brozzetti, G. Pomposo, G. Lavecchia, D. Di Naccio, and F. Ferrarini (2010), Coseismic ground deformation of the 6 April 2009 L'Aquila earthquake (central Italy, Mw6.3), *Geophys. Res. Lett.*, *37*, L06308, doi:10.1029/2010GL042807.

Bonnefoy-Claudet, S., S. Baize, L. F. Bonilla, C. Berge-Thierry, C. Pasten, J. Campos, P. Volant, and R. Verdugo (2009), Site effect evaluation in the basin of Santiago de Chile using ambient H/V measurements, *Geophys. J. Int.*, *176*, 925–937, doi:10.1111/j.1365-246X.2008.04020.x.

Bosi, C., F. Galadini, B. Giaccio, P. Messina, and A. Sposato (2003), Plio-Quaternary continental deposits in the Latium-Abruzzi Apennines: The correlation of geological events across different intermontane basins, *Il Quaternario*, *16*(1Bis), 55–76.

Boué, P., M. Denolle, N. Hirata, S. Nakagawa, and G. C. Beroza (2016), Beyond basin resonance: Characterizing wave propagation using a dense array and the ambient seismic field, *Geophys. J. Int.*, *206*(2), 1261–1272, doi:10.1093/gji/ggw205.

Castellaro, S., and F. Mulargia (2009), The effect of velocity inversions on H/V, *Pure Appl. Geophys.*, *166*(4), 567–592, doi:10.1007/s00024-009-0474-5.

Cavinato, G. P., and P. G. De Celles (1999), Extensional basins in the tectonically bimodal central Apennines fold-thrust belt, Italy: Response to corner flow above a subducting slab in retrograde motion, *Geology*, *27*(10), 955–958, doi:10.1130/0091-7613(1999)027<0955:EBITTB>2.3.CO;2.

Cesi, C., M. Di Filippo, M. Di Nezza, and M. Ferri (2010), Caratteri gravimetrici della media Valle del Fiume Aterno, in *Microzonazione sismica per la ricostruzione dell'area aquilana*, vol. 3, Gruppo di Lavoro MS–AQ Ed., Regione Abruzzo –Dipartimento della Protezione Civile, L'Aquila.

Chaljub, E., P. Moczo, S. Tsuno, P.-Y. Bard, J. Kristek, M. Kaser, M. Stupazzini, and M. Kristekova (2010), Quantitative comparison of four numerical predictions of 3D ground motion in the Grenoble valley, France, *Bull. Seismol. Soc. Am.*, *100*(4), 1427–1455.

Chiarabba, C., L. Jovane, and R. Di Stefano (2005), A new view of Italian seismicity using 20 years of instrumental recordings, *Tectonophysics*, *305*, 251–268, doi:10.1016/j.tecto.2004.09.013.

Chiaraluce, L. (2012), Unravelling the complexity of Apenninic extensional fault systems: A review of the 2009 L'Aquila earthquake (Central Apennines, Italy), *J. Struct. Geol.*, *42*, 2–18, doi:10.1016/j.jsg.2012.06.007.

Chiaraluce, L., L. Valoroso, D. Piccinini, R. Di Stefano, and P. De Gori (2011), The anatomy of the 2009 L'Aquila normal fault system (central Italy) imaged by high resolution foreshock and aftershock locations, *J. Geophys. Res.*, *116*, B12311, doi:10.1029/2011JB008352.

Christiansen, A. V., and E. Auken (2012), A global measure for depth of investigation, *Geophysics*, *77*, 171–177, doi:10.1190/GEO2011-0393.1.

Christiansen, A. V., E. Auken, and K. Sørensen (2009), The transient electromagnetic method, in *Groundwater Geophysics*, pp. 179–226, Springer, Berlin.

Christiansen, A. V., E. Auken, and A. Viezzoli (2011), Quantification of modeling errors in airborne TEM caused by inaccurate system description, *Geophysics*, *76*, 43–52, doi:10.1190/1.3511354.

Cinti, F. R., D. Pantosti, P. M. De Martini, S. Pucci, R. Civico, S. Pierdominici, L. Cucci, C. A. Brunori, S. Pinzi, and A. Patera (2011), Evidence for surface faulting events along the Paganica fault prior to the 6 April 2009 L'Aquila earthquake (central Italy), *J. Geophys. Res.*, *116*, B07308, doi:10.1029/2010JB007988.

Civico, R., S. Pucci, D. Pantosti, and P. M. De Martini (2015), Morphotectonic analysis of the long-term surface expression of the 2009 L'Aquila earthquake fault (Central Italy) using airborne LiDAR data, *Tectonophysics*, doi:10.1016/j.tecto.2014.12.024.

Cowie, P. A., and G. P. Roberts (2001), Constraining slip rates and spacings for active normal faults, *J. Struct. Geol.*, *23*, 1901–1915, doi:10.1016/S0191-8141(01)00036-0.

D'Agostino, N., F. Speranza, and R. Funiciello (1997), Le Brecce Mortadella dell'Appennino Centrale: Primi risultati di stratigrafia magnetica, *Il Quaternario*, *10*, 385–388.

D'Agostino, N., S. Mantenuto, E. D'Anastasio, R. Giuliani, M. Mattome, S. Calcaterra, P. Gambino, and L. Bonci (2011), Evidence for localized active extension in the central Apennines (Italy) from global positioning system observations, *Geology*, *39*(4), 291–294, doi:10.1130/G31796.1.http://hdl.handle.net/2122/7049.

Danielsen, J. E., E. Auken, F. Jørgensen, V. H. Søndergaard, and K. I. Sørensen (2003), The application of the transient electromagnetic method in hydrogeophysical surveys, *J. Appl. Geophys.*, *53*, 181–198, doi:10.1016/j.jappgeo.2003.08.004.

De Luca, G., S. Marcucci, G. Milana, and T. Sano (2005), Evidence of low-frequency amplification in the city of L'Aquila, Central Italy, through a multidisciplinary approach including strong-and weak-motion data, ambient noise, and numerical modelling, *Bull. Soc. Seismol. Am.*, *95*(4), 1469–1481.

Delgado, J., C. L. Casado, J. Giner, A. Estevez, A. Cuenca, and S. Molina (2000), Microtremors as a geophysical exploration tool: Applications and limitations, *Pure Appl. Geophys.*, *157*, 1445–1462.

Di Giulio, G., G. R. de Nardis, P. Boncio, G. Milana, G. Rosatelli, F. Stoppa, and G. Lavecchia (2016), Seismic response of a deep continental basin including velocity inversion: The Sulmona intermontane basin (Central Apennines, Italy), *Geophys. J. Int.*, *204*(1), 418–439, doi:10.1093/gji/ggv444.

Di Giulio, G., I. Gaudiosi, F. Cara, G. Milana, and M. Tallini (2014), Shear-wave velocity profile and seismic input derived from ambient vibration array measurements: The case study of downtown L'Aquila, *Geophys. J. Int.*, *198*(2), 848–866, doi:10.1093/gji/ggu162.

Effersø, F., E. Auken, and K. I. Sørensen (1999), Inversion of band-limited TEM responses, *Geophys. Prospect.*, *47*, 551–564, doi:10.1046/j.1365-2478.1999.00135.x.

Field, E. H., and K. H. Jacob (1995), A comparison and test of various site response estimation techniques, including three that are not reference site dependent, *Bull. Seismol. Soc. Am.*, *85*, 1127–1143.

Flores-Estrella, H., S. Yussim, and C. Lomnitz (2006), Seismic response of the Mexico City Basin: A review of twenty years of research, *Nat. Hazards*, *40*, 357–372, doi:10.1007/s11069-006-0034-6.

Galadini, F., and P. Galli (2000), Active tectonics in the Central Apennines (Italy)—Input data for seismic hazard assessment, *Nat. Hazards*, *22*, 225–270, doi:10.1023/A:1008149531980.

Galadini, F., and P. Messina (2004), Early–middle Pleistocene eastward migration of the Abruzzi Apennine (central Italy) extensional domain, *J. Geodyn.*, *37*(1), 57–81, doi:10.1016/j.jog.2003.10.002.

Galli, P., B. Giaccio, and P. Messina (2010), The 2009 central Italy earthquake seen through 0.5 Myr-long tectonic history of the L'Aquila faults system, *Quat. Sci. Rev.*, *29*, 3768–3789, doi:10.1016/j.quascirev.2010.08.018.

Galli, P. A. C., B. Giaccio, P. Messina, E. Peronace, and G. M. Zuppi (2011), Palaeoseismology of the L'Aquila faults (central Italy, 2009, Mw 6.3 earthquake): Implications for active fault linkage, *Geophys. J. Int.*, *187*, 1119–1134, doi:10.1111/j.1365-246X.2011.05233.x.

García-Jerez, A., F. Luzón, M. Navarro, and J. Pérez-Ruiz (2006), Characterization of the sedimentary cover of the Zafarraya Basin, Southern Spain, by means of ambient H/V, *Bull. Seismol. Soc. Am.*, *96*, 957–967, doi:10.1785/0120050061.

Garofalo, F., et al. (2016), InterPACIFIC project: Comparison of invasive and non-invasive methods for seismic site characterization. Part I: Intra-comparison of surface wave methods, *Soil Dyn. Earthquake Eng.*, *82*, 222–240.

Gawthorpe, R. L., and M. R. Leeder (2000), Tectono-sedimentary evolution of active extensional basins, *Basin Res.*, *12*, 195–218, doi:10.1111/j.1365-2117.2000.00121.x.

Ghisetti, F., and L. Vezzani (1991), Thrust belt development in the central Apennines: Northward polarity of thrusting and out-of-sequence deformation in the Gran Sasso chain (Italy), *Tectonics*, *10*, 904–919, doi:10.1029/91TC00902.

Giaccio, B., P. Galli, P. Messina, E. Peronace, G. Scardia, G. Sottili, A. Sposato, E. Chiarini, B. Jicha, and S. Silvestri (2012), Fault and basin depocentre migration over the last 2 Ma in the L'Aquila 2009 earthquake region, central Italian Apennines, *Quat. Sci. Rev.*, *56*(2012), 69–88, doi:10.1016/j.quascirev.2012.08.016.

Giocoli, A., P. Galli, B. Giaccio, V. Lapenna, P. Messina, E. Peronace, S. Piscitelli, and G. Romano (2011), Electrical Resistivity Tomography across the Paganica-San Demetrio fault system (April 2009 L'Aquila earthquake, Mw 6.3), *B. Geofis. Teor. Appl.*, *52*, 457–469, doi:10.4430/bgta0029.

Gold, C. M. (1989), Surface Interpolation, spatial adjacency and GIS, in *Three Dimensional Applications in Geographic Information Systems*, edited by J. Raper, pp. 21–35, Taylor and Francis, London.

Goldman, M., L. Tabarovsky, and M. Rabinovich (1984), On the influence of 3-D structures in the interpretation of transient electromagnetic sounding data, *Geophysics*, *59*, 889–901.

Graves, R. W., A. Pitarka, and P. G. Somerville (1998), Ground-motion amplification in the Santa Monica area: Effects of shallow basin-edge structure, *Bull. Seismol. Soc. Am.*, *88*(5), 1224–1242.

Group, E. W. (2010), Evidence for surface rupture associated with the Mw 6.3 L'Aquila earthquake sequence of April 2009 (central Italy), *Terra Nova*, *22*(1), 43–51, doi:10.1111/j.1365-3121.2009.00915.x.

Guéguen, P., C. Cornou, S. Garambois, and J. Banton (2007), On the limitation of the H/V spectral ratio using seismic H/V as an exploration tool: Application to the Grenoble valley (France), a small apex ratio basin, *Pure Appl. Geophys.*, *164*(1), 115–134.

Hartzell, S., A. L. Leeds, L. Ramirez-Guzman, J. P. Allen, and R. G. Schmitt (2016), Seismic site characterization of an urban sedimentary basin, Livermore Valley, California: Site response, basin-edge-induced surface waves, and 3D simulations, *Bull. Seismol. Soc. Am.*, *106*(2), 609–631, doi:10.1785/0120150289.

Hengl, T. (2006), Finding the right pixel size, *Comput. Geosci.*, *32*(9), 1283–1298, doi:10.1016/j.cageo.2005.11.008.

Herrmann, R. B., L. Malagnini, and I. Munafò (2011), Regional moment tensors of the 2009 L'Aquila earthquake sequence, *Bull. Seismol. Soc. Am.*, *101*(3), 975–993, doi:10.1785/0120100184.

Hinzen, K. G., F. Scherbaum, and B. Weber (2004), On the resolution of H/V measurements to determine sediment thickness, a case study across a normal fault in the Lower Rhine Embayment, Germany, *J. Earthquake Eng.*, *8*(6), 909–926.

Horike, M. (1996), Geophysical exploration using microtremor measurements, in *Proc. of the 11th World Conf. on Earthquake Eng., Acapulco, Mexico*, 2033.

Hunstad, I., G. Selvaggi, N. D. Agostino, P. England P. Clarke, and M. Pierozzi (2003), Geodetic strain in peninsular Italy between 1875 and 2001, *Geophys. Res. Lett.*, *30*(4), 1181, doi:10.1029/2002GL016447.

Ibs-Von Seht, M., and J. Wohlenberg (1999), Microtremor measurements used to map thickness of soft sediments, *Bull. Seismol. Soc. Am.*, *89*(1), 250–259.

Improta, L., et al. (2012), High-resolution controlled-source seismic tomography across the Middle Aterno basin in the epicentral area of the 2009, Mw 6.3, L'Aquila earthquake (central Apennines, Italy), *Ital. J. Geosci.*, *131*(3), 373–388, doi:10.3301/IJG.2011.35.

Istituto Superiore per la Protezione e la Ricerca Ambientale (ISPRA) (2006), foglio 359 L'Aquila. Carta Geologica d'Italia alla scala 1:50000, S.EL. CA., Firenze, Italy.

Konno, K., and T. Ohmachi (1998), Ground-motion characteristics estimated from spectral ratio between horizontal and vertical components of microtremors, *Bull. Seismol. Soc. Am.*, *88*(1), 228–241.

Lachet, C., and P.-Y. Bard (1994), Numerical and theoretical investigations on the possibilities and limitations of Nakamura's technique, *J. Phys. Earth*, *42*(5), 377–397.

Langston, C., and S. Horton (2014), Three-dimensional seismic-velocity model for the unconsolidated Mississippi Embayment sediments from H/V ambient H/V measurements, *Bull. Seismol. Soc Am.*, *104*(5), 2349–2358.

Lavecchia, G., F. Brozzetti, M. R. Barchi, J. Keller, and M. Menichetti (1994), Seismotectonic zoning in east-central Italy deduced from the analysis of the Neogene to present deformations and related stress fields, *Bull. Geol. Soc. Am.*, *106*, 1107–1120, doi:10.1130/0016-7606(1994)106<1107:SZIECI>2.3.CO;2.

Lavecchia, G., F. Ferrarini, F. Brozzetti, R. De Nardis, P. Boncio, and L. Chiaraluce (2012), From surface geology to aftershock analysis: Constraints on the geometry of the L'Aquila 2009 seismogenic fault system, *Ital. J. Geosci.*, *131*(3), 330–347, doi:10.3301/IJG.2012.24.

Le Roux, O., C. Cornou, D. Jongmans, and S. Schwartz (2012), 1-D and 2-D resonances in an Alpine valley identified from ambient H/V measurements and 3-D modelling, *Geophys. J. Int.*, *191*(2), 579–590.

Leeder, M. R., and R. L. Gawthorpe (1987), Sedimentary models for extensional tilt-block/half-graben basins, *Geol. Soc. London, Spec. Publ.*, *28*, 139–152, doi:10.1144/GSL.SP.1987.028.01.11.

Lunedei, E., and P. Malischewsky (2015), A review and some new issues on the theory of the H/V technique for ambient vibrations, in *Perspectives on European Earthquake Engineering and Seismology*, vol. 2, edited by A. Ansal, pp. 371–394, Springer International Publishing, Cham (ZG), Switzerland.

Macrì, P., A. Smedile, F. Speranza, L. Sagnotti, M. Porreca, T. Mochales, and E. Russo Ermolli (2016), Analysis of a 150 m sediment core from the co-seismic subsidence depocenter of the 2009 Mw = 6.1 L'Aquila earthquake (Italy): Implications for Holocene-Pleistocene tectonic subsidence rates and for the age of the seismogenic Paganica fault system, *Tectonophysics*, *687*, 180–194, doi:10.1016/j.tecto.2016.09.004.

McNeill, J. D., M. Bosnar, and G. M. Levy (1984), Application of simple loop to the interpretation of transient electromagnetic surveys in a resistive environment, Geonics Limited, *Tech. Note* TN-12, 1-13.

Michel, C., B. Edwards, V. Poggi, J. Burjánek, D. Roten, C. Cauzzi, and D. Fäh (2014), Assessment of site effects in Alpine regions through systematic site characterization of seismic stations, *Bull. Seismol. Soc. Am.*, *104*(6), 2809–2826, doi:10.1785/0120140097.

Montone, P., M. T. Mariucci, and S. Pierdominici (2012), The Italian present-day stress map, *Geophys. J. Int.*, *189*, 705–716, doi:10.1111/j.1365-246X.2012.05391.x.

Moro, M., S. Gori, E. Falcucci, M. Saroli, F. Galadini, and S. Salvi (2013), Historical earthquakes and variable kinematic behaviour of the 2009 L'Aquila seismic event (central Italy) causative fault, revealed by paleoseismological investigations, *Tectonophysics*, *583*, 131–144.

MS–AQ Working Group (2010), Microzonazione sismica per la ricostruzione dell'area aquilana. Regione Abruzzo—Dipartimento della Protezione Civile, L'Aquila, 1–796 (in Italian). [Available at: http://www. protezionecivile.gov.it/jcms/it/view_pub.wp?contentId=PUB25330, last accessed April 2016.]

Nabighian, M. N., and J. C. Macnae (1991), Appendix A: TEM systems, in *Electromagnetic Methods in Applied Geophysics*, vol. II, edited by M. N. Nabighian, pp. 479–483, Newmont Exploration Limited, Denver, Colo.

Nakamura, Y. (1989), A method for dynamic characteristics estimation of subsurface using microtremor on the ground surface, *Railway Tech. Res. Inst. Quart. Rep.*, *30*(1), 25–33.

Nakamura, Y. (2000), Clear identification of fundamental idea of Nakamura's technique and its applications, in 12th World Conf. on Earthquake Engineering, Auckland, New Zealand.

Newman, G. A., G. W. Hohmann, and W. A. Anderson (1986), Transient electromagnetic response of a three-dimensional body in a layered Earth, *Geophysics*, *51*, 1608–1627.

Nicol, A., J. J. Walsh, J. Watterson, and J. R. Underhill (1997), Displacement rates of normal faults, *Nature*, *390*, 157–169, doi:10.1038/36548.

Nogoshi, M., and T. Igarashi (1971), On the amplitude characteristics of microtremor (Part 2), *J. Seismol. Soc. Jpn*, *24*, 24–60.

Overduin, P. P., C. Haberland, T. Ryberg, F. Kneier, T. Jacobi, M. N. Grigoriev, and M. Ohrnberger (2015), Submarine permafrost depth from ambient seismic H/V, *Geophys. Res. Lett.*, *42*, 7581–7588, doi:10.1002/2015GL065409.

Palacky, G. J. (1987), Resistivity characteristics of geologic targets, in *Electromagnetic Methods in Applied Geophysics*, vol. 1, edited by M. N. Nabighian, pp. 53–129, Society of Exploration Geophysicists, Tulsa, Okla.

Patacca, E., R. Sartori, and P. Scandone (1990), Tyrrhenian Basin and Apenninic Arcs: Kinematic relations since late Tortonian times, *Mem. Soc. Geol. Ital.*, *45*, 425–451.

Piña-Flores, J., M. Perton, A. García-Jerez, E. Carmona, F. Luzón, J. Molina-Villegas, and F. Sánchez-Sesma (2016), The inversion of spectral ratio H/V in a layered system using the diffuse field assumption (DFA), *Geophys. J. Int.*, *208*(1), 577–588, doi:10.1093/gji/ggw416.

Pitarka, A., K. Irikura, T. Iwata, and H. Sekiguchi (1998), Three-dimensional simulation of the near-fault ground motion for the 1995 Hyogo-Ken Nanbu (Kobe), Japan, earthquake, *Bull. Seismol. Soc. Am.*, *88*(2), 428–440.

Pizzi, A., and F. Galadini (2009), Pre-existing cross-structures and active fault segmentation in the northern-central Apennines, *Tectonophysics*, *476*, 304–319, doi:10.1016/j.tecto.2009.03.018.

Podvin, P., and I. Lecomte (1991), Finite difference computation of traveltimes in very contrasted velocity model: A massively parallel approach and its associated tools, *Geophys. J. Int.*, *105*, 271–284.

Porreca, M., et al. (2016), Geological reconstruction in the area of maximum co-seismic subsidence during the 2009 Mw = 6.1 L'Aquila earthquake using geophysical and borehole data, *Ital. J. Geosci.*, doi:10.3301/IJG.2015.37.

Pucci, S., F. Villani, R. Civico, D. Pantosti, A. Smedile, P. M. De Martini, D. Di Naccio, and A. Gueli (2014), Morphotectonic, Quaternary and structural geology Analyses of the shallow geometry of the Mw 6.1, 2009 L'Aquila earthquake fault (central Italy): A missed opportunity for surface faulting prevention, Abstract T22C-08 Fall Meeting, AGU. [Available at http://abstractsearch.agu.org/meetings/2014/FM/T22C-08.html.]

Pucci, S., F. Villani, R. Civico, D. Pantosti, P. Del Carlo, A. Smedile, P. M. De Martini, E. Pons-Branchu, and A. Gueli (2015), Quaternary geology map of the Middle Aterno Valley, 2009 L'Aquila earthquake area (Abruzzi Apennines, Italy), *J. Maps*, doi:10.1080/17445647.2014.927128.

Pucci, S., et al. (2016), Deep electrical resistivity tomography along the tectonically active Middle Aterno Valley (2009 L'Aquila earthquake area, central Italy), *Geophys. J. Int.*, *207*(2), 967–982.

Revil, A., et al. (2011), Hydrogeology of Stromboli volcano, Aeolian Islands (Italy) from the interpretation of resistivity tomograms, self-potential, soil temperature and soil CO2 concentration measurements, *Geophys. J. Int.*, *186*(3), 1078–1094, doi:10.1111/j.1365-246X.2011.05112.x.

Roten, D., D. Fäh, C. Cornou, and D. Giardini (2006), Two-dimensional resonances in Alpine valleys identified from ambient vibration wavefields, *Geophys. J. Int.*, *165*(3), 889–905, doi:10.1111/j.1365-246X.2006.02935.x.

Rovida, A., R. Camassi, P. Gasperini, and M. Stucchi (2011), CPTI11, the 2011 version of the Parametric Catalogue of Italian Earthquakes, Milano, Bologna, last release 2011-12-23, http://emidius.mi.ingv.it/CPTI, doi:10.6092/INGV.IT-CPTI11.

Salloum, N., D. Jongmans, C. Cornou, D. Massih, F. Chehade, C. Voisin, and A. Mariscal (2014), The shear wave velocity structure of the heterogeneous alluvial plain of Beirut (Lebanon): Combined analysis of geophysical and geotechnical data, *Geophys. J. Int.*, *199*(2), 894–913, doi:10.1093/gji/ggu294.

Sambridge, M., J. Braun, and H. (1995), Geophysical parameterization and interpolation of irregular data using natural neighbours, *Geophys. J. Int.*, *122*, 837–857, doi:10.1111/j.1365-246X.1995.tb06841.x.

Sánchez-Sesma, F. J., M. Rodríguez, U. Iturrarán-Viveros, A. Rodríguez-Castellanos, M. Suárez, M. A. Santoyo, A. García-Jerez, and F. Luzón (2010), Site effects assessment using seismic H/V, In Proc. of the 9th Int. Workshop on Seismic Microzoning and Risk Reduction, 21–24.

Sánchez-Sesma, F. J., M. Rodríguez, U. Iturrarán-Viveros, F. Luzón, M. Campillo, L. Margerin, A. García-Jerez, M. Suárez, M. A. Santoyo, and A. Rodríguez-Castellanos (2011), A theory for microtremor H/V spectral ratio: Application for a layered medium, *Geophys. J. Int.*, *186*(1), 221–225.

Sapia, V., A. Viezzoli, A. Menghini, M. Marchetti, and M. Chiappini (2015), The Italian reference site for TEM methods, *Ann. Geophys.*, *58*(5, G0548), doi:10.4401/ag-6805.

Santucci de Magistris, F., et al. (2013), Geotechnical characterization of the Aterno Valley for site response analysis, in *Rivista Italiana di Geotecnica* Anno XLVII, vol. n. 3, pp. 23–43 , Pàtron Editore, Bologna.

Scognamiglio, L., E. Tinti, A. Michelini, D. S. Dreger, A. Cirella, M. Cocco, S. Mazza, and A. Piatanesi (2010), Fast determination of moment tensors and rupture history: What has been learned from the 6 April 2009 L'Aquila earthquake sequence, *Seismol. Res. Lett.*, *81*(6), 892–906, doi:10.1785/gssrl.81.6.892.

Semblat, J. F., M. Kham, E. Parara, P. Y. Bard, K. Pitilakis, K. Makra, and D. Raptakis (2005), Site effects: Basin geometry vs soil layering, *Soil Dyn. Earthquake Eng.*, *25*(7), 529–538.

Sibson, R. (1981), A brief description of natural neighbour interpolation, in *Interpreting Multivariate Data*, edited by V. Barnett, pp. 21–36, Wiley, New York, USA.

Tallini, M., G. Cavuoto, F. Del Monaco, V. Di Fiore, M. Mancini, G. Caielli, G. P. Cavinato, R. De Franco, N. Pelosi, and A. Rapolla (2012), Seismic surveys interated with geological data for in-depth investigation of Mt. Pettino active Fault area (Western l'Aquila Basin), *Ital. J. Geosci.*, *131*(3), 389–402, doi:10.3301/IJG.2012.10.

Tertulliani, A., A. Rossi, L. Cucci, and M. Vecchi (2009), L'Aquila (central Italy) earthquakes: The predecessors of the April 6, 2009 event, *Seismol. Res. Lett.*, *80*(6), 1008–1013, doi:10.1785/gssrl.80.6.1008.

Tokimatsu, K. (1995), Geotechnical Site Characterization using Surface Waves. In Proc. First International Conference on Earthquake Geotechnical Engineering, IS-Tokyo '95, Tokyo, November 14–16, Balkema, Rotterdam, 1333-1368.

Uebayashi, H. (2003), Extrapolation of irregular subsurface structures using the horizontal-to-vertical ratio of long-period microtremors, *Bull. Seismol. Soc. Am.*, *93*(2), 570–582.

Valensise, G., and D. Pantosti (2001), The investigation of potential earthquake sources in peninsular Italy: A review, *J. Seismolog.*, *5*, 287, doi:10.1023/A:1011463223440.

Valoroso, L., L. Chiaraluce, D. Piccinini, R. Di Stefano, D. Schaff, and F. Waldhauser (2013), Radiography of a normal fault system by 64,000 high-precision earthquake locations: The 2009 L'Aquila (central Italy) case study, *J. Geophys. Res. Solid Earth*, *118*, 1156–1176, doi:10.1002/jgrb.50130.

Vannoli, P., P. Burrato, U. Fracassi, and G. Valensise (2012), A fresh look at the seismotectonics of the Abruzzi (Central Apennines) following the 6 April 2009 L'Aquila earthquake (Mw 6.3), *Ital. J. Geosci.*, *131*(3), 309–329, doi:10.3301/IJG.2012.03.

Vezzani, L., and F. Ghisetti (1998), Carta Geologica dell'Abruzzo, Scala 1:100,000, S.EL.CA., Firenze.

Villani, F., et al. (2015), Imaging the structural style of an active normal fault through multi-disciplinary geophysical investigation: A case study from the Mw 6.1, 2009 L'Aquila earthquake region (central Italy), *Geophys. J. Int.*, doi:10.1093/gji/ggu462.

Villani, F., L. Improta, S. Pucci, R. Civico, P. Bruno, and D. Pantosti (2017), Investigating the architecture of the Paganica Fault (2009 Mw 6.1 earthquake, central Italy) by integrating high-resolution multi-scale refraction tomography and detailed geological mapping, *Geophys. J. Int.*, *208*(1), 403–423, doi:10.1093/gji/ggw407.

Vittori, E., et al. (2011), Surface Faulting of the 6 April 2009 Mw 6.3 L'Aquila Earthquake in Central Italy, *Bull. Seismol. Soc. Am.*, *101*(4), 1507–1530, doi:10.1785/0120100140.

Wathelet, M., D. Jongmans, and M. Ohrnberger (2004), Surface-wave inversion using a direct search algorithm and its application to ambient vibration measurements, *Near Surf. Geophys.*, *2*, 211–221.

Wells, D. L., and K. J. Coppersmith (1994), New empirical relationships among magnitude, rupture length, rupture width, rupture area, and surface displacement, *Bull. Seismol. Soc. Am.*, *84*(4), 974–1002.

Westaway, R. (1991), Continental extension in set of parallel faults: Observational evidence and theoretical models, *Geol. Soc. London, Spec. Publ.*, *1991*(56), 143–169, doi:10.1144/GSL.SP.1991.056.01.10.

Yamanaka, H., M. Takemura, H. Ishida, and M. Niwa (1994), Characteristics of long-period microtremors and their applicability in exploration of deep sedimentary layers, *Bull. Seismol. Soc. Am.*, *84*, 1831–1841.